BN SA 518

INTERIM REPORT

EXPERIMENT DEFINITION STUDIES FOR AMPS SPACELAB

NASA/MSFC CONTRACT NAS8-31415

Principal Investigator:
Harold Liemohn

Physics and Instrumentation Department
Math and Physics Research Section

December 1975

Battelle
Pacific Northwest Laboratories
Richland, WA 99352

BN SA 518

INTERIM REPORT

EXPERIMENT DEFINITION STUDIES FOR AMPS SPACELAB

NASA/MSFC CONTRACT NAS8-31415

Principal Investigator:
Harold Liemohn

Physics and Instrumentation Department
Math and Physics Research Section

December 1975

Battelle
Pacific Northwest Laboratories
Richland, WA 99352

INTERIM REPORT

EXPERIMENT DEFINITION STUDIES FOR AMPS SPACELAB

TABLE OF CONTENTS

ELECTRICAL CHARGING OF SHUTTLE ORBITER

by

H. B. Liemohn

BATTELLE
Pacific Northwest Laboratories
Richland, Washington 99352

December 1975

Interim Report to
National Aeronautics and Space Administration
George C. Marshall Space Flight Center
MSFC, AL 35812

NASA/MSFC Contract NAS8-31415

ELECTRICAL CHARGING OF SHUTTLE ORBITER

by

H. B. Liemohn

ABSTRACT

The Space Shuttle Orbiter has the geometrical configuration of an aircraft and nonconducting outer skin that is expected to generate considerable transient charging and local potential differences due to the ambient ionospheric plasma. Emission of high-current electron beams has been proposed for the AMPS Spacelab payload that would induce large potentials and return currents to the Orbiter skin. Quantitative estimates are presented for the magnitude and transient behavior for both the passive and active conditions.

A comprehensive model of the Orbiter environment has been defined that includes the ambient ionospheric medium at a nominal altitude of 400 km and the neutral gas cloud expelled by the vehicle. The outer skin of the vehicle is covered with ~ 1300 m^2 of thermal insulation which has the dielectric quality of air and ~ 60 m^2 of metal surfaces on rocket motors and exposed instrumentation on the Spacelab pallet. Local equilibrium potentials for passive conditions have been calculated for various ion, electron, and photon shadow zones. These potentials vary from -3.3 volts where only electrons and insulator leakage current are present to +3.9 volts where only ion ram current is collected. Potential differences of only a few volts between adjacent insulation tiles or at sharp corners can produce local electric fields of 10 kV/m or more.

The theory for induced charging of spacecraft due to operation of electron guns has only been developed for spherical metal vehicles and constant emission currents, which are not directly applicable to

to the Orbiter situation. Field-aligned collection of electron return current from the ambient ionosphere provides up to ~150 ma on the conducting surfaces and ~2.4 amps on the dielectric thermal insulation. Local ionization of the neutral atmosphere by energetic electron bombardment or electrical breakdown provides somewhat more return current. Differential charging between the dielectric insulator skin and the internal conductors causes high potentials and electric fields across the insulation. Estimates of the transient behavior and potential magnitude are obtained by solving electric circuit analogies. For gun currents of 10 amps, the conductor potential appears to be in the range 10^3 - 10^5 volts depending on the induced external ionization of the vehicle atmosphere. A more thorough analysis of the plasma sheath dynamics during electron gun pulses is needed to refine this extimate of the Orbiter potential.

Active methods for increasing the collection of electron return current include tethered balloons to enhance the conductor collection area, electron beam ionization of special neutral gas clouds, and simultaneous operation of the VLF antenna to enhance the electron sheath. The feasibility of these techniques is presently under study by other contractors.

Electrical charging of spacecraft in the ionosphere and magnetosphere is a consequence of different fluxes of thermal electrons and ions striking the surface of the vehicle. Normally a very small equilibrium potential is established over the skin of the vehicle which does not affect the operation of sensors and electronic instrumentation. However, the Space Shuttle Orbiter has unusual characteristics that are expected to cause considerable transient charging, larger than normal electrical potentials, and significant localized electric fields that may have serious consequences for operation of sensitive instruments. Furthermore, the AMPS Spacelab payload presents additional requirements that may generate extreme potentials unless remedial steps are taken to counteract the flow of electrical charge.

The Orbiter may acquire appreciable charge differentials and local electric fields due to its large airplane shape and its nonconducting outer skin. As the vehicle assumes different attitudes in the course of its mission, various outer surfaces will be shadowed from particle and/or photon bombardment. Owing to alignment of charged-particle trajectories along the geomagnetic field and the relatively large difference in electron and ion speeds, there are many more regions of the spacecraft surface that are accessible to electrons than to ions. In addition, the photoemission of electrons from the surface by solar ultraviolet will depend on spacecraft attitude. Thus, the local current flow to the skin of the vehicle will vary widely from point to point. The dielectric skin of the vehicle prevents rapid flow of surface current to neutralize the differential charging and as a consequence potential differences and attendant electric fields may be anticipated. During normal passive operations of the vehicle, potential differences of several volts are expected between adjacent areas of the vehicle where the surface contour changes abruptly (edges of wings, payload bay door edges, and around corners).

Operation of active experiments is expected to include ejection of large amounts of electrical charge in the form of electron beams that must be

compensated by a return current to the vehicle. Relatively slow collection of return electron current from the ambient ionosphere prevents rapid charge neutralization of the electron-beam charge. Proposed gun currents of, say, 1 ampere for 100 milliseconds are predicted to cause transient excursions of the vehicle potential may exceed many thousands of volts unless appropriate compensating return current is available.

Since operation of an electron gun at keV energies from the AMPS Spacelab is a vital part of the overall mission objective, it is imperative to find some method for holding the transient potentials in check. Among the possibilities are a conducting balloon tethered to the vehicle that can collect return electron current at a rate equal to the gun current. Another possibility is beam ionization of a neutral gas cloud that would provide many free electrons for return current collection. A third alternative is to operate the long VLF antenna simultaneously to form a large electron sheath from which to draw return current. In the evaluation of these prospective methods, the time lag between the injected current and the return current collection is a vital consideration because it will determine the magnitude of the potential transient.

The published literature on ambient charging of spacecraft in the ionosphere and magnetosphere is quite thorough for vehicles with conducting outer skin. Only a few papers have treated the problem of large electron current ejection from spacecraft, and their applicability to a realistic pulsed mode of operation is open to question. The Shuttle Orbiter presents additional complications due to its nonconducting outer skin which can only be discharged by the ambient plasma medium. For example, an electron gun pulse will drive the skin potential positive until enough return current is collected to neutralize the overall potential of the vehicle, but by that time the skin will have built up a negative charge which must be neutralized by ion bombardment, photoemission, and conduction leakage to the interior structure. This complicated problem has not been studied heretofore.

The purpose of the present investigation is to delineate the physics of Shuttle Orbiter charging and discharging during operation of the electron gun. The level-of-effort supported by this contract to date has not

permitted detailed modeling of the vehicle potential. However, most important aspects of the problem have been surveyed, and specific avenues for more thorough investigation have been identified.

A. Ambient Spacecraft Environment

The Shuttle Orbiter that carries the AMPS Spacelab is scheduled to operate at a nominal altitude of approximately 400 km (250 miles). A model of the ionospheric environment has been defined for this nominal Orbiter altitude in order to provide a consistent basis for comparison of spacecraft charging and discharging calculations. Key model parameters for the charged constituents, the neutral constituents, and the resulting plasma properties are pesented in the accompanying tables. The numerical values were selected by the author as representative of typical ambient conditions that will be encountered by the spacelab missions. They represent a composite of estimates found in several aeronomy reference books (Johnson, 1965; Hanson, 1965; Rishbeth and Garriott, 1969; Kasha, 1969; Whitten and Poppoff, 1971; and Banks and Kockarts, 1973).

The charged constituents at F-region altitudes consist principally of oxygen ions and electrons and their properties are summarized in Table 1. Large variations in both density and temperature for these constituents are attributed to source and transport mechanisms that vary diurnally as well as with season and solar cycle. An important consequence of the constituent temperatures is the fact that the spacecraft speed is considerably greater than the mean thermal speed of the ions but significantly less than the mean thermal speed of electrons. This has important consequences for current collection by particle flux at the vehicle skin. The mean velocity components perpendicular and parallel to the local geomagnetic field were calculated for an isotropic (Maxwellian) distribution. Collisional scattering of the particles is due principally to long range coulomb forces by the atomic oxygen ions; neutral gas scattering and charge exchange is negligible at these altitudes. The relatively broad range of values for the mean free path is attributable to both density and particle speed variations. A nominal gyroradius was calculated for a geomagnetic field of 0.4 Gauss which represents a mean value for the early low-inclination orbits. Since the

TABLE 1. Nominal Ionospheric Environment--Charged Conctituents

Shuttle Orbit: Z_s = 400 km, V_s = 7.7 km/sec, T_s = 5250 sec = 88 min

OXYGEN ION O^+ (90%)	ELECTRON e^- (100%)
$N_i = 2 \times 10^{11}$ m^{-3}	$N_e = 2 \times 10^{11}$
(Day: $2 \times 10^{11} - 10^{12}$ m^{-3}; Night:	$7 \times 10^{10} - 5 \times 10^{11}$ m^{-3})
T_i = 1000 °K (0.09 ev)	Te = 2500 °K (0.22 ev)
(700 - 1500°K)	(1500 - 3500 °K)
$\overline{V}_i$ = 1.2 km/sec (0.15 V_s)	$\overline{V}_e$ = 300 km/sec (39 V_s)
$\overline{V}_{i\perp}$ = 0.98 km/sec; $\overline{V}_{i\parallel}$	$\overline{V}_{e\perp}$ = 244 km/sec; $\overline{V}_{e\parallel}$
$\overline{V}_{e\parallel}$ = 0.69 km/sec	$\overline{V}_{e\parallel}$ = 173 km/sec
ν_i^{coll} = 0.2 sec^{-1} (O^+, N^+)	ν_e^{coll} = 300 sec^{-1} (O^+, N^+)
λ_i^{mfp} = 6 km	λ_e^{mfp} = 1.0 km
(2 - 20 km)	(0.3 - 2 km)
r_i^B (0.4G) = 4.2 m	r_e^B (0.4G) = 0.033 m
$N_i V_s = 1.5 \times 10^{15}$ m^{-2} sec^{-1}	$N_e \overline{V}_{e\parallel} = 3.5 \times 10^{16}$ m^{-2} sec^{-1}
$M = 2.67 \times 10^{-27}$ kgm	$m = 9.1 \times 10^{-31}$ kgm

ions are effectively stationary with respect to the spacecraft and the spacecraft is effectively stationary with respect to the electron motion, the particle currents describe the ion flux in the ram direction and the electron flux on a surface normal to the local geomagnetic field.

At the Shuttle Orbiter altitude the primary neutral constituent in the ionosphere is atomic oxygen, which has properties shown in Table 2. Again a wide range of gas characteristics are encountered due to diurnal, seasonal, and solar effects. Most atomic oxygen parameters are comparable with those for ionic oxygen except that the neutral density is three orders of magnitude greater. Around the Shuttle Orbiter, outgassing of skin materials significantly enhances the background neutral gas density; estimates of its magnitude are presented in the next section.

The plasma properties displayed in Table 3 also vary over a range of values, as they are derived from parameter values for the neutral and charged constituents. Evidently the electron cyclotron frequency is nearly always less than the plasma frequency. The Debye length of the plasma is only about 1 centimeter which represents a scale length for shielding of externally applied potentials in the steady-state situation. For a spacecraft that cuts across geomagnetic field lines and is subject to transient potential excursions, the Debye length does not adequately describe the scale of nonneutrality, but is retained as a convenient distance parameter. In a plasma medium which is subject to a static magnetic field, current flow due to an electric field is anisotropic and conductivity of the medium is described by a tensor. When the elctric field is parallel to the magnetic field, magnetic effects on the conductivity may be ignored (σ_0). When the electric field is orthogonal to the static magnetic field, the current flow is sharply reduced by many orders of magnitude. The Pedersen conductivity (σ_1) is in the direction of the orthogonal electric field, and the Hall conductivity (σ_2) is in a direction perpendicular to both the applied electric field and the static magnetic field. This conduction anistropy severely limits the collection of return current on the spacecraft, since *the current flow is restricted to field aligned directions unless very large electric fields are generated.*

TABLE 2. Nominal Ionospheric Environment--Neutral Constituents

Shuttle Orbit: Z_s = 400 km, V_s = 7.7 km/sec, T_s = 5250 sec = 88 min

OXYGEN ATOM O (90%)

M_n = 16 amu

(14 - 20)

$N_n = 2 \times 10^{14}\ m^{-3}$

(10^{13} - $7 \times 10^{14}\ m^{-3}$)

T_n = 1000 °K

(700 - 1500 °K)

$\overline{V}_n$ = 1.2 km/sec

$\nu_{n\ coll} = 0.12\ sec^{-1}$

λ_n^{mfp} = 10 km

(3 - 200 km)

TABLE 3. Nominal Ionospheric Environment--Plasma Properties

Shuttle Orbit: Z_s = 400 km. V_s = 7.7 km/sec, T_s = 5250 sec = 88 min

f_B (0.4G) = 1100 kHz

(800 - 1800 kHz)

f_p = 4000 kHz

(1500 - 10000 kHz)

λ_{Debye} = 0.008 m

(0.004 - 0.012 m)

($N_e \lambda_D^3 = 10^5$)

σ_0 = 20 mhos/m ($\parallel$ B, $\parallel$ E)

(5 - 30 mhos/m)

$\sigma_1 = 2 \times 10^{-7}$ mhos/m ($\perp$B, $\parallel$ E)

(10^{-8} - 10^{-6} mhos/m)

$\sigma_2 = 6 \times 10^{-10}$ mhós/m ($\perp$B, $\perp$ E)

(10^{-11} - 10^{-8} mhos/m)

It must be emphasized that the tabular entries are representative of a nominal ionospheric environment and do not always describe the medium adjacent to the spacecraft skin. For example, as indicated above, outgassing of the skin may alter the neutral gas cloud around the vehicle appreciably, particularly following shutdown of the main rocket engines after orbit insertion or during attitude maneuvers when control thrusters are fired. Another significant source of local gas is periodic evaporation of water vapor from the fuel cells. Electrical circuitry in the Shuttle Orbiter is expected to produce a rather strong electromagnetic noise component that will affect the ambient magnetic field direction near the vehicle, and may affect the equilibrium configuration of electric fields on the skin. Large electric fields on the outer skin during electron-gun operation are expected to ionize the neutral gas and modify the plasma density and collision frequencies adjacent to the vehicle. Thus, the tensor conductivity of the plasma medium around the vehicle is expected to be somewhat higher than the ambient model environment. Some of these effects will be considered in following sections.

B. Surface Properties of Orbiter/AMPS Spacelab

The outer surface of the Shuttle Orbiter and the AMPS Spacelab is almost entirely nonconducting electrically. This is a consequence of the requirement for a good thermal insulator on the outer surface to accommodate reentry heating. Low thermal conductivity and high electrical conductivity are incompatible qualities of the surface materials that are currently planned for the Orbiter skin. The nonconducting outer skin poses some unusual electrical problems for the operation of certain AMPS Spacelab experiments. In this subsection the properties of the outer skin materials that affect spacecraft charging are summarized.

Less than 5% of the outer surface of the Shuttle Orbiter/AMPS Spacelab consists of good metallic conducter. More than 90% of the surface consists of good thermal insulating material that has extremely high electrical resistivity (10^{17} x the resistance of a good metal conducter). The dielectric constant of these thermal insulators is comparable to that of air; consequently, they are capable of withstanding potentials of several thousand volts between the outer skin and the internal metallic structure of the vehicle. Such potentials are not expected across the insulation material, although significant voltage drops (100's volts) are anticipated during operation of the electron gun in the AMPS Spacelab payload. Differential charging of local regions on the skin produces local electric fields parallel to the skin that can be appreciable (1000's volts/m), however, and coronal arcing at surface boundary gaps is conceivable.

The exterior surface of the Shuttle Orbiter consists of various types of reusable thermal insulation materials (insulation data provided by Mr. John Lobb, NASA/JSC, Houston, in private communications) as shown in Figure 1. The top surfaces (wings, bay doors) are largely coated nomex felt (FRSI) illustrated in Figure 2. The low-temperature insulation (LRSI) is located on upper surfaces that may encounter some heating during reentry (upper fuselage and vertical stabilizer); its internal structure and bonding are illustrated in Figure 3. The entire underside (fuselage and wings) is covered with high-temperature insulation (HRSI) which is relatively thick (up to 10 cm) to protect the internal structure from reentry heat; its

NASA-S-75-6069

WA
SEPTEMBER 1975

ORBITER THERMAL PROTECTION SYSTEM

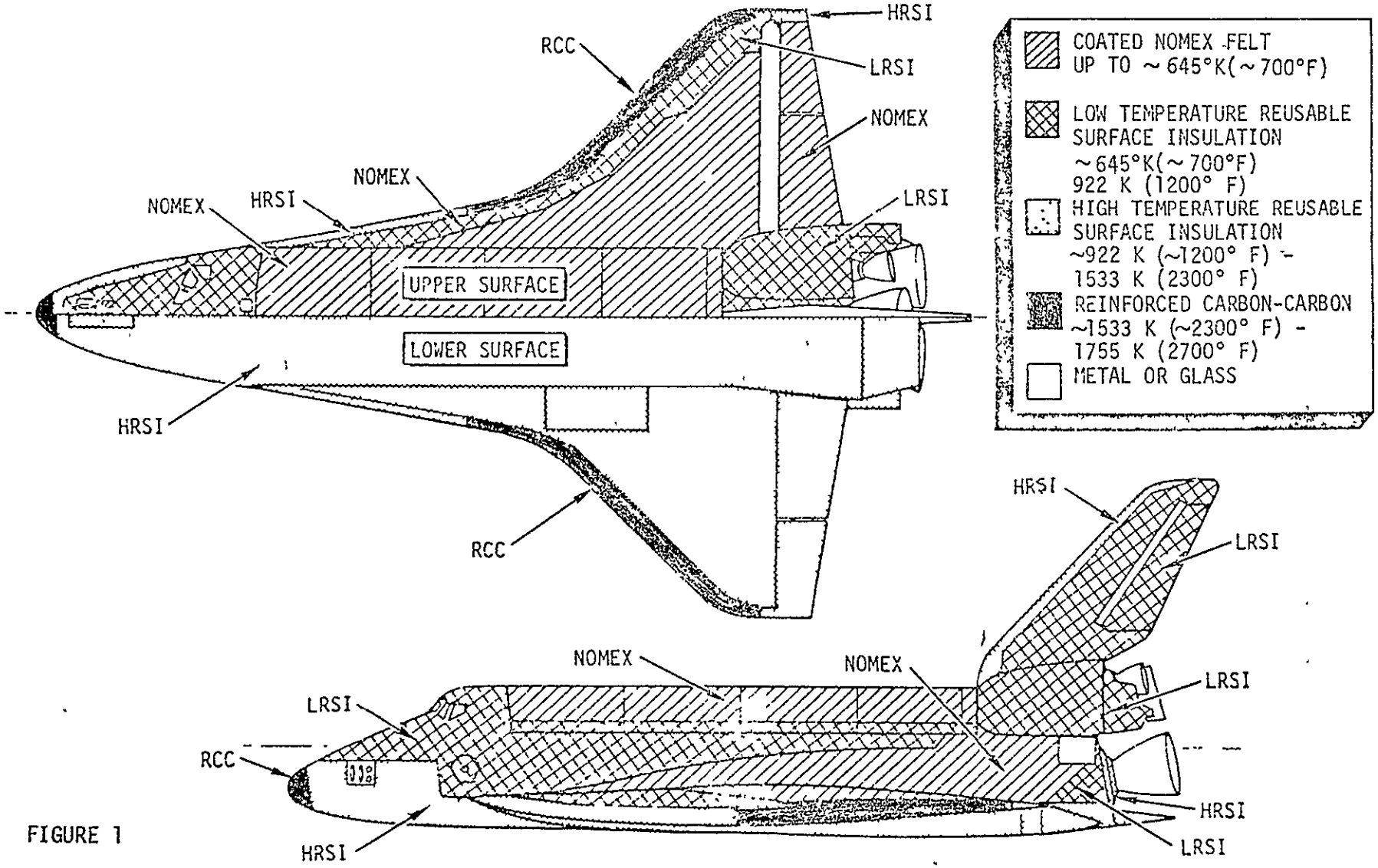

FIGURE 1

F R S I

FLEXIBLE REUSABLE SURFACE INSULATION

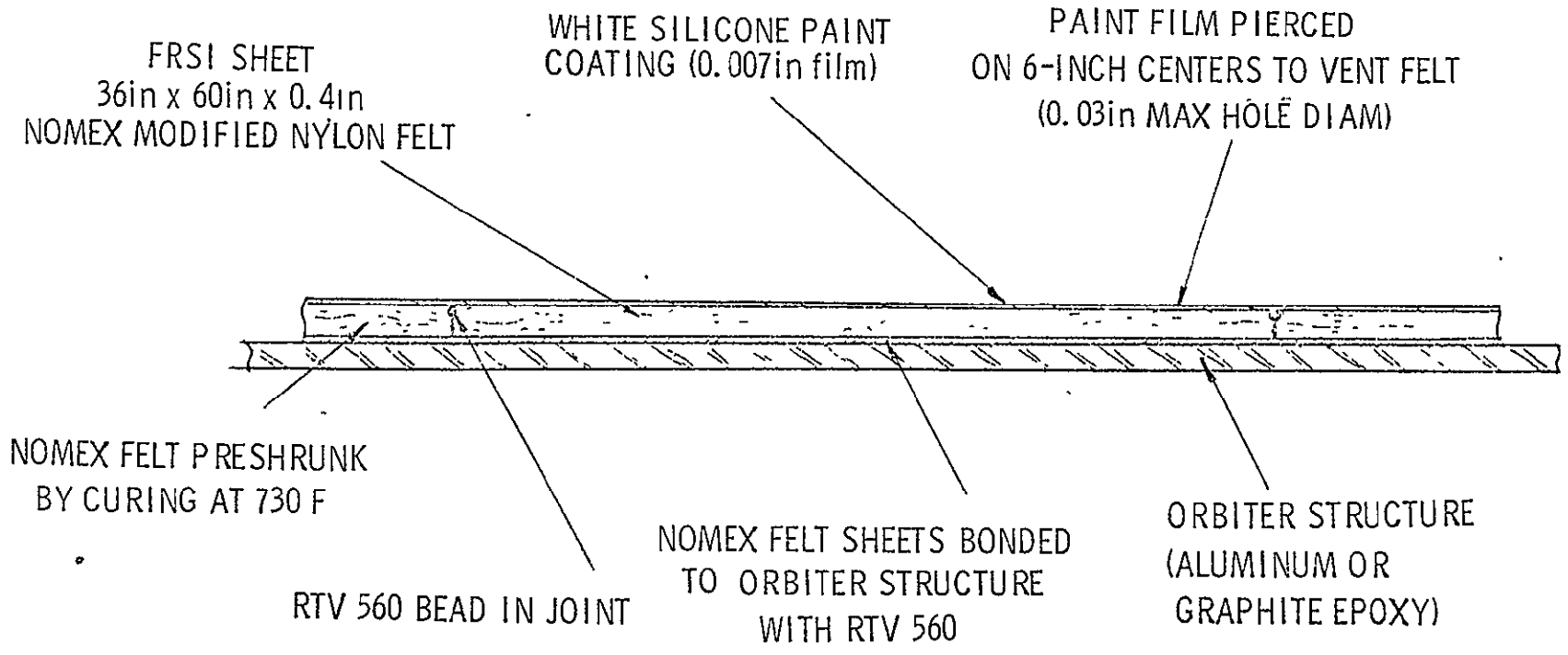

FIGURE 2

L R S I

LOW TEMPERATURE REUSABLE SURFACE INSULATION

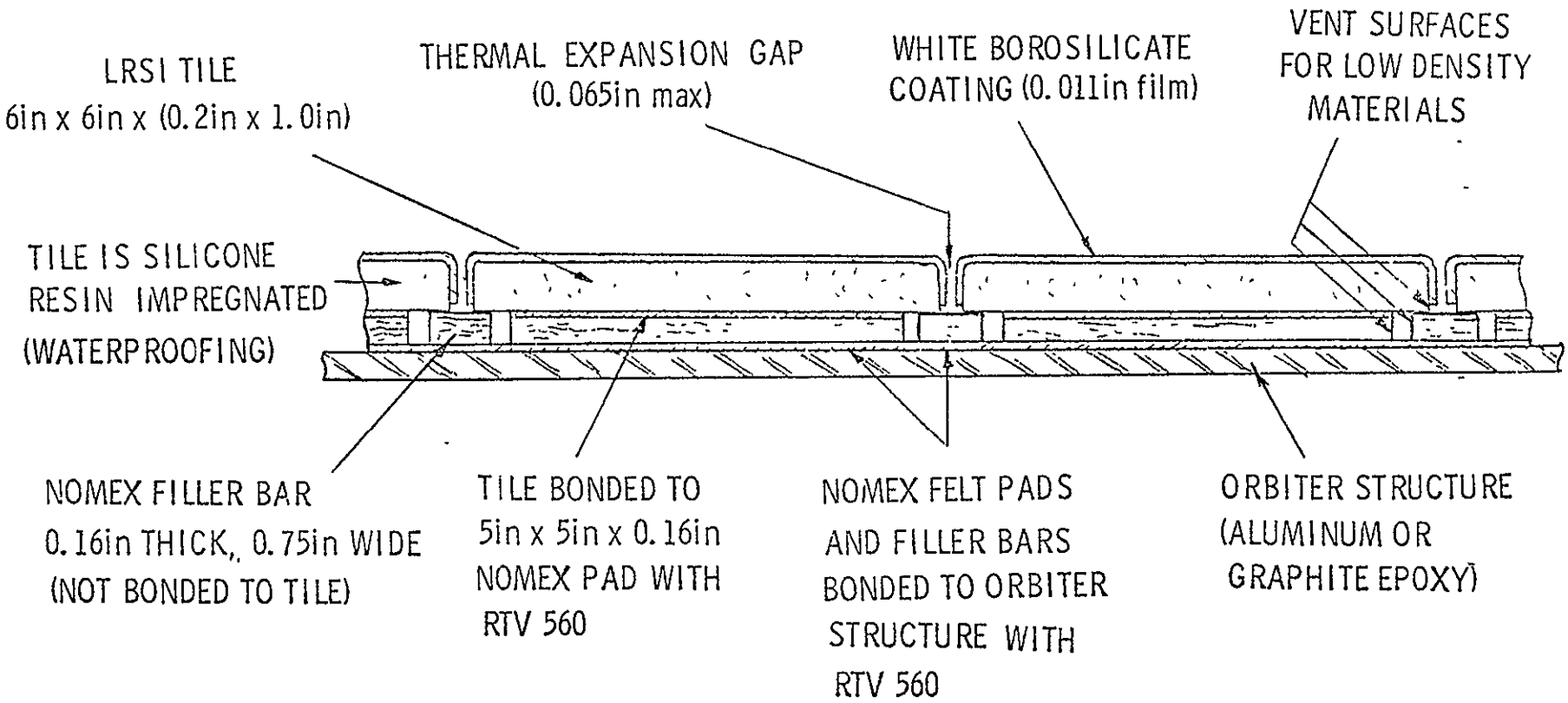

FIGURE 3

HRSI

HIGH TEMPERATURE REUSABLE SURFACE INSULATION

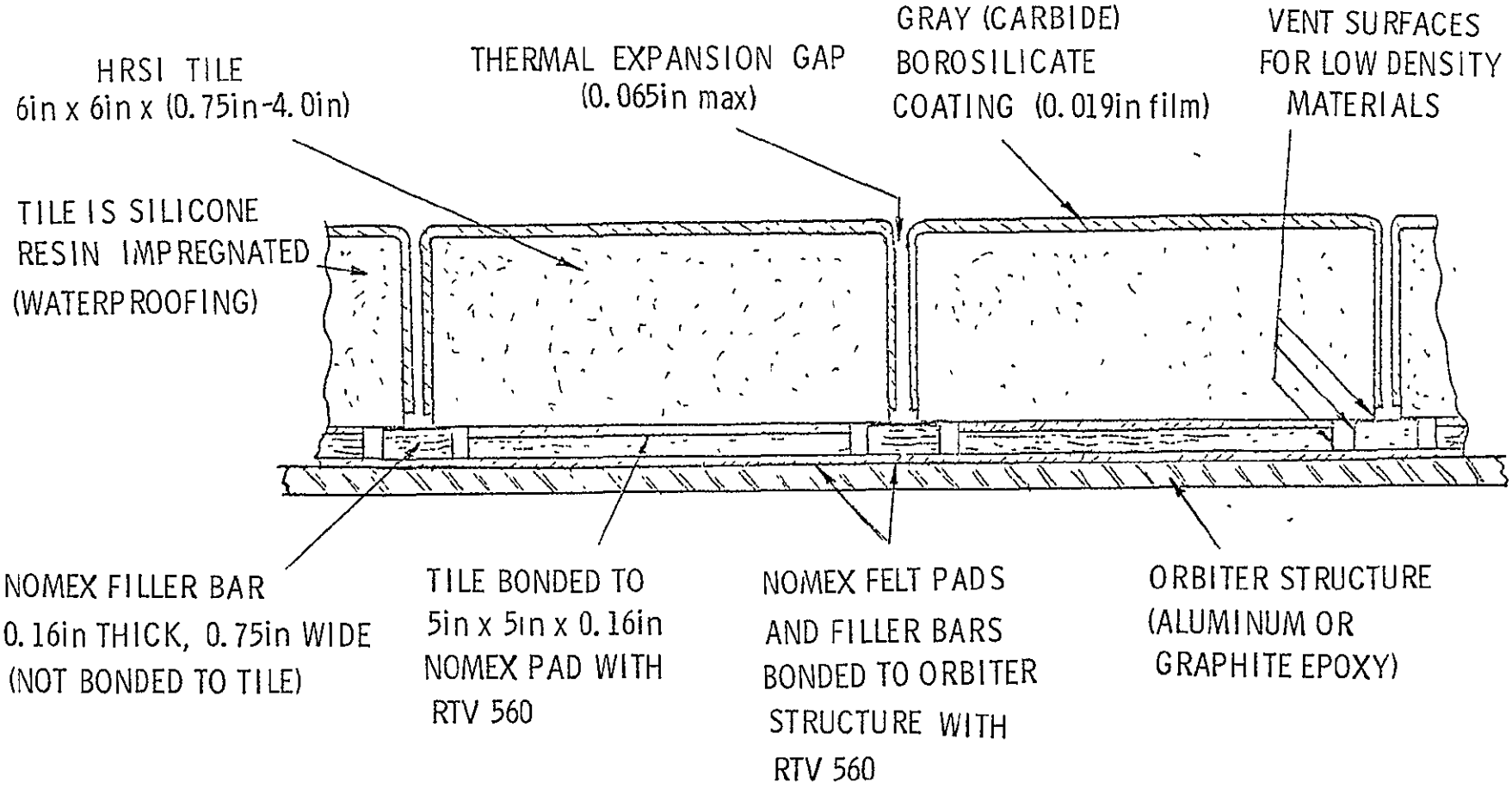

FIGURE 4

construction is displayed in Figure 4. For particularly high temperature areas (nose and wing leading edges) reinforced carbon-carbon (RCC) is used.

The "soft" insulation materials (FRSI, LRSI, and HRSI) are made of silicone impregnated with resin to provide water proofing. The nomex (FRSI) is used alone and as backing for the other insulation tiles. The entire layer of insulation materials is bonded with RTV 560 and overcoated with a thin layer of borosilicate. Individual 15 cm square tiles (LRSI and HRSI) are spaced about 0.2 mm apart to allow for thermal expansion during reentry. All of the insulation materials (except RCC) are effusive sources of neutral gas when subjected to the rigors of the space environment.

There are some metallic exterior surfaces that provide "shorted" electrical contact between the interior metal structure of the Orbiter and the external plasma. The location of these good conductors is illustrated in Figure 5. The primary area is provided by the metal rocket motor nozzles. Other substantial surface areas are provided by the antenna boom, pallet instruments, and the manipulator arm. Since the pallet is graphite epoxy which is a poor conductor, there is some question about the electrical contact between these latter instrument related conductors and the Orbiter superstructure. In view of the high electrical power planned for some experiments, it is imperative that these structures be properly grounded. For purposes of the present analysis, all of the external metal surfaces are assumed to be in direct contact with each other and the internal superstructure.

The electrical properties of the primary external surfaces of the Orbiter/AMPS-Spacelab are tabulated in Table 4. The foregoing thermal materials are excellent electrical insulators, with a dielectric permittivity of air. The exterior metal surfaces are, of course, excellent conductors. Of special interest for scientific researchers is the lack of an effective external ground plane; the Spacelab pallet and control room have graphite epoxy exterior surfaces which are not conductors. Overall, the metal surfaces amount to about 60 m^2 whereas nonconductor surfaces cover 1300 m^2.

AMPS SHUTTLE ORBITER ELECTRICAL CONDUCTING SURFACES

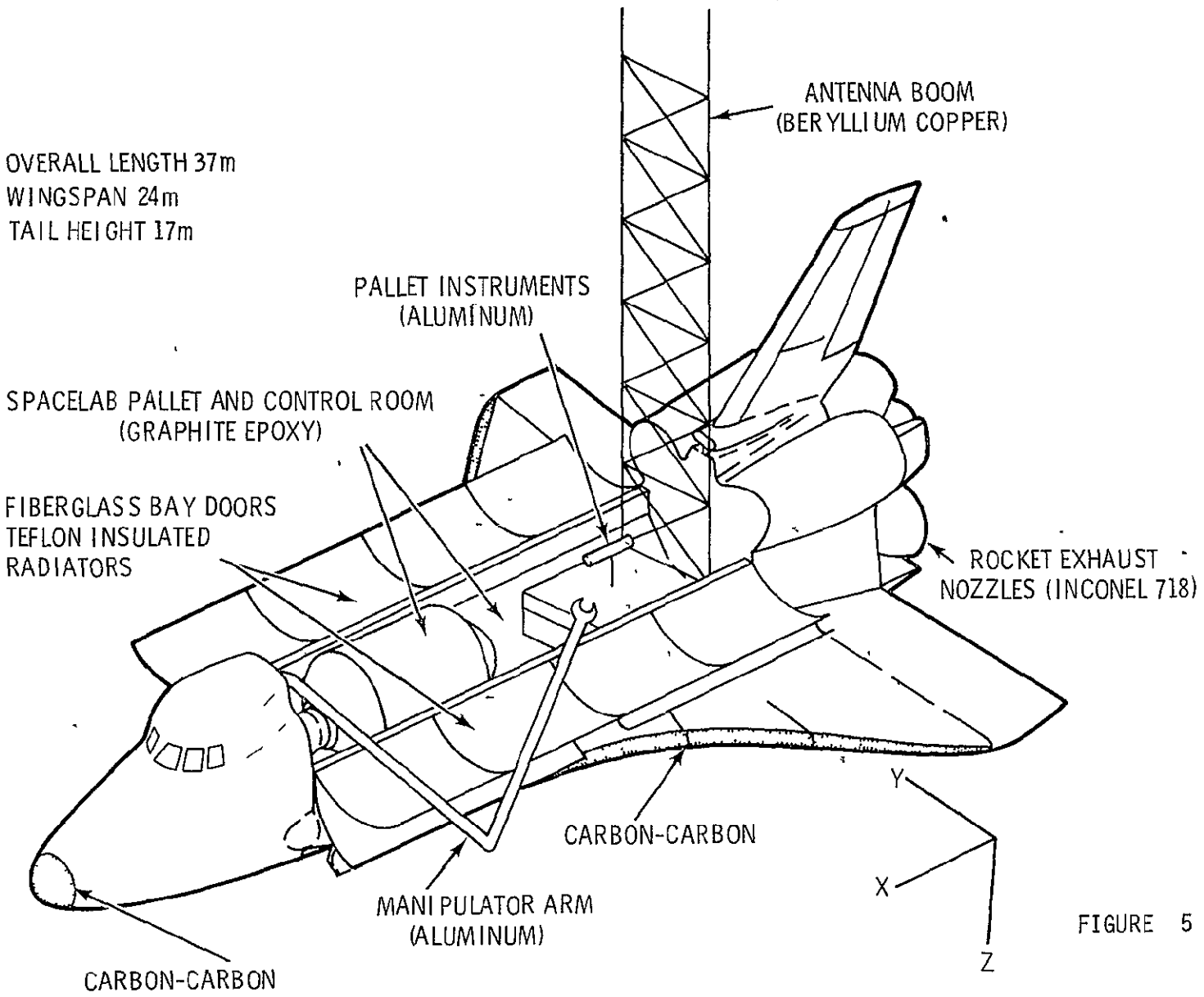

FIGURE 5

TABLE 4. Orbiter/AMPS-Spacelab Outer Skin Materials

Location	Material	Area $Meters^2$	Thickness Meters	Electrical Conductivity mhos/m	Dielectric Constant κ
Topside (low temp.)	FRSI	300	0.011	10^{-10}	∿1
Topside (high temp.)	LRSI	280	0.010 - 0.030	10^{-9}-10^{-10}	∿1
Underside (reentry shield)	HRSI	475	0.024-0.107	10^{-9}-10^{-10}	∿1
Nose and Wing Edge	RCC	37.5	0.006	10^{-6}	∿1
Rocket Exhaust Nozzles	Inconel 718	∿30	--	6×10^{6}	--
Interior Bay Door Radiators	Teflon	∿100	--	10^{-10}	∿1
Spacelab Pallet	Graphite Epoxy	∿90	--	10^{-10}	∿1
Spacelab Control Room	Graphite Epoxy	∿25	--	10^{-10}	∿1
Spacelab Pallet Instruments	Aluminum	∿10	--	3×10^{7}	--
Antenna Boom	Beryllium Copper	15	--	1×10^{7}	--
Manipulator Arm	Aluminum	5	--	3×10^{7}	--

The thermal insulation does conduct a small amount of electric current through its fibrous interior as well as over its surface. For some external conditions or modes of experimental operation, this conduction from the internal structure is vital to establish equilibrium. Under most situations, however, the thermal blanket acts as a dielectric capacitor which efficiently stores charge on its external surfaces. The capacitance and resistance of the blanket per unit area are $\kappa\varepsilon_0/\Delta h$ and $\Delta h/\sigma$, respectively, where κ is the relative dielectric constant, ε_0 is the permittivity of free space (8.85 $\mu\mu$f/m), σ is the electrical conductivity, and Δh is the blanket thickness. The e-folding time constant for discharging such an electrical circuit is

$$\tau_{RC} = \kappa\varepsilon_0/\sigma$$

According to Table 4, this discharge constant is 0.01 - 0.1 sec for the thermal blanket. The total area of the thermal blanket gives an overall capacitance of 0.5 μf and an overall resistance of 2×10^4 to 2×10^5 ohms using an average blanket thickness of 2.5 cm.

There is considerable neutral gas released by the Shuttle Orbiter that may contaminate its natural environment. Passive releases from the outer skin materials, cabin atmosphere leakage, and active exhausting from vernier rockets and fuel-cells provide localized enhancements of the neutral gas around the vehicle. A comprehensive study of contamination control has recently been completed for NASA (Rantanen and Ress, 1975). Results obtained here are based on the conclusions in this report.

Characteristics of the five major sources of gas contamination are presented in Table 5 (from Rantanen and Ress, 1975, Table I, p. 50). Outgassing is the steady release of heavy molecules from the nonmetallic skin materials exposed to the vacuum environment of space. Offgassing is the prompt release of adsorbed volatile species primarily from the nonmetallic materials. There are two flash evaporator vents near the rear of the fuselage that periodically expel large amounts of water vapor from the fuel cells. Cabin atmosphere

TABLE 5. Major Sources of Neutral Gas Emissions from the Shuttle Orbiter (after Rantanen and Ress, 1975)

Major Sources	Duration/ Frequency	Flowrate ***	Constituents	Plume Shape Function ***	Velocity ***	Size Parameter
Outgassing	Continuous	$\left[5.0e^{-t/4100}\ e^{(T-100)/29} \times 10^{-10}\right]$ g/cm^2/sec	Hydrocarbon chain fragments RTV's, etc.	$\cos\theta / r^2$	$12.9\sqrt{T}$ m/sec	Molecular Avg. M = 100
Offgassing	Continuous for first 100 hours on-orbit	$\left[3.87e^{-0.14t} + 3.0e^{-.055t}\right] e^{(T-100)/29} \times 10^{-9}$ g/cm^2/sec	Water light gases Volatiles	$\cos\theta / r^2$	$30.4\sqrt{T}$ m/sec	Molecular Avg. M = 18
Evaporator (2) *	As Reqd.	13.6 kg/hr total	Water	$\cos^6(1.01\,\theta)/r^2$ $[0° \leq \theta \leq 36.8°]$ $\frac{e^{-.0773(\theta-36.8°)}}{r^2}$ $[36.8° < \theta \leq 148°]$	1012 m/sec	Molecular M = 18
Cabin Atmosphere Leakage	Continuous	3.18 kg/day	O_2 N_2 CO_2 H_2O	$\cos\theta / r^2$	$2220\sqrt{\frac{1}{M}}$ m/sec	Molecular Avg. M = 29
RCS Vernier Engines**	As Reqd.	40.8 g/min Avg. 40 msec pulse ea. 4.8 sec--Y-POP attitude at 200 km	H_2O N_2 H_2 CO CO_2 H	$\frac{(\cos\frac{\pi}{2}\frac{\theta}{\theta_i})^{8.65}}{r^2}$ $[0° \leq \theta \leq 40°]$ $\frac{e^{.0467(\theta-40°)}}{r^2}$ $[40° < \theta \leq 140°]$ $\frac{e^{-4.67}}{r^2}$ $[140° < \theta \leq 180°]$	3505 m/sec	Molecular
Ambient Reflection	~10 to 30 min per orbit	Varies with above sources & orbital attitude	Any of the above sources	$\cos\theta/r^2$ from collision points	Varies with all above sources Max = 7.65 km/sec	Varies with all above sources

* Plume reflections off of structural surfaces (e.g. wings, experiment bay doors) are equivalent to a source equal to the plume impingement rate with a $\cos\theta/r^2$ distribution and a velocity of $30.4\sqrt{T}$ m/sec from the surface where T = surface temp.

** RCS plume reflections off of structural surfaces are assumed to have a rate equal to the plume impingement rate with a $\cos\theta/r^2$ distribution and a velocity equal to $129\sqrt{\frac{T}{M}}$ where T = surface temperature.

*** Dimensions are included implicitly. Flowrate has t in hours and T in degrees centigrade; Velocity has T in degrees Kelvin, and Plume Shape Function uses r in centimeters.

leaks from various seals around doors, windows, and other ports. Finally, there are six 25 lb (nominal) thrust vernier control rocket engines that are used for vehicle attitude control. Curiously, outgassing of the main rocket engine following orbit insertion is not treated in the study although it may be a significant source during the early hours of the mission.

The shape of the gas cloud and its local density distribution can be estimated for the data in Table 5. (Expressions in this table must be evaluated cautiously; for the flowrate, t is in hours and T is in degrees centigrade, whereas for the velocity, T is in degrees Kelvin and M is the molecular mass number.) The plume shape function ($\cos^n / r^2$ with r in centimeters) is legitimate only for point sources. For distributed sources like outgassing and offgassing, this form applies to locally uniform areas as a whole, and adjacent to these surfaces the density is locally uniform. Angular dependence is important at discontinuous boundaries. The evaporators, cabin leakage, and vernier engines are essentially point sources so that their exhausts obey their plume shape functions adjacent to the vehicle. Another important consideration in determining the plume density distribution is the mean free path of the gas molecules. For the parameter ranges of interest, the molecular mean free path is inversely proportional to the total gas density. A relatively short mean free path would significantly alter the plume shape by diffusion.

The foregoing considerations are incorporated into the gas density estimates presented in Table 6. For numerical estimates the skin temperature is assumed to be 80°C on sunlit surfaces (from 20°C on FRSI to 100°C on HRSI and metal) and -120°C on nonsunlit surfaces (from -100 to -130°C). Since the neutral gas does not slow down appreciably as it leaves the vehicle, the density is given by flowrate/velocity. The gas cloud moves with the vehicle as well, since collisions with the ambient ionosphere are relatively rare compared to intra cloud molecular collisions. For outgassing and offgassing estimates, the vehicle is equivalent to a sphere of radius a = 10m; (surface area 1300m^2) and the density falls off as a^2/r^2 at large distances. Angular dependence ($\cos\theta$) is important when combining distributions from sunlit and nonsunlit surfaces. For the point sources, the radial falloff scales

TABLE 6. Plume Gas Densities (molecules/m^3)

Source	Time in Orbit			Remarks
	8 hrs	24 hrs	72 hrs	
Outgassing (sunlit 80°C)	6×10^{13}	6×10^{13}	6×10^{13}	These densities are approximately uniform above uniformly illuminated surfaces. Radially they scale as $(10 \text{ meters})^2 / r^2(m)$ in the range 10 m to 10 km. At thermal and geometric discontinuities the different source regions have cos θ angular dependence.
Outgassing (nonsunlit - 120°C)	1×10^{10}	1×10^{10}	1×10^{10}	
Offgassing (sunlit 80°C)	9×10^{14}	3×10^{14}	1.7×10^{13}	
Offgassing (nonsunlit -120°C)	1.4×10^{12}	4×10^{11}	2.6×10^{10}	

	Radial Distance on Axis (θ = 0°)				
	1 cm	10 cm	1 m	10 m	
Evaporations	1.3×10^{24}	1.3×10^{22}	1.3×10^{20}	1.3×10^{18}	Angular variation $\cos^6 \theta$; Continuous up to 5 hours
Cabin Leakage	1.8×10^{22}	1.8×10^{20}	1.8×10^{18}	1.8×10^{16}	Angular variation cos θ; Continuous
Vernier Engines	2.2×10^{24}	2.2×10^{22}	2.2×10^{20}	2.2×10^{18}	Peak density in 40 msec pulse. Average M ~18

as r^{-2} where r is in centimeters. Beyond distances of the order of the ambient mean free path (10 km), the plume is dispersed and falls behind as part of the vehicle wake.

Comparison of the ambient oxygen density from Table 2 with the outgassing and offgassing densities in Table 6 shows that the Shuttle Orbiter is generating its own atmosphere. The local density on the sunlit side of the vehicle is of the same order as the ambient oxygen ($10^{14}/m^3$). The nonsunlit side is virtually filled in by sunlit emissions with cosθ angular degradation. The low values on the nonsunlit side are only appropriate near the vehicle (well inside 10 m).

The evaporators, cabin leakage and vernier engines produce narrow rayed plumes that are several orders of magnitude denser than ambient. More importantly, the mean free path is extremely short (0.1 mm at $10^{22}/m^3$ to 1m at $10^{18}/m^3$) so that the molecules in these plumes undergo many collisions. Presumably this collisional dispersion is taken into account in the empirical angular factors (although cosθ for cabin leakage is purely geometrical). In general, these exhaust plumes move radially away from the vehicle and do not contribute appreciably to the total density adjacent to the skin.

One notable exception that will be useful later to neutralize the electron charge is the evaporator plume location. Several vent locations are under consideration, but the most likely position is about 1 m above the trailing edge of each wing. The plume axes are presumably aligned parallel with the trailing edge of the wing. Thus, very high gas densities (10^4 - 10^6 times ambient) are available adjacent to the vehicle skin at a sharp discontinuity during operation of the gun. Some vernier engine exhaust plumes also strike surfaces of the vehicle, but these attitude controls would presumably be shut down during electron gun operations.

C. Ambient Spacecraft Potentials

Any material surface that is in contact with a plasma of ions and electrons will attain an equilibrium electrical potential that is slightly different than the plasma potential. The potential difference is due to the random thermal motion of the ambient ions and electrons which produces a larger flux of electrons than ions impinging on the surface. In general these potentials are very small since the thermal energy density is low (0.1 - 10 electron volts), but it can be much larger at geosychronous altitude. At the Shuttle orbit the ionospheric plasma has a modest thermal energy according to Table 1, and potential differences of only a few volts on the skin of the vehicle are anticipated due to the ambient medium.

Calculation of spacecraft potentials has been treated extensively in the open literature, and steady-state solutions for passive vehicles with conducting outer skins are summarized in two review books (Al'pert, Gurevich, and Pitaevskii, 1965; and Kasha, 1969). The results that have been reported are restricted to relatively simple geometries, usually a spherical satellite, so that some caution is advised in their application to the Shuttle Orbiter charging problem.

To illustrate the collection of particle current on the vehicle skin, consider electrons impinging on an electrically neutral plane surface of width W and length L. Since electrons are sharply confined to gyration about field lines ($r_e^B \sim 3$ cm), their principal microscopic motron is parallel to $\underline{B}$ with a mean velocity component $\overline{V}_{e\parallel}$. To simplify geometry, $\overline{V}_{e\parallel}$ is assumed to be normal to the plane surface which is moving at satellite speed V_s in the plane of the surface. In a time interval Δt, the electron current I_e hitting the top of the surface comes from the volume $(V_s \Delta t\ W)\ \overline{V}_{e\parallel}\ \delta t$, where $\delta t = L/V_s$ is the maximum available travel time for the electron to reach the plane surface before the trailing edge of the surface has passed by the field line. The height of the ambient collection volume above the surface is, therefore, $H = \overline{V}_{e\parallel}\ \delta t = 2OL$. The

total charge collected in Δt from a plasma with uniform density N_e is

$$I_e \Delta t = -e \frac{N_e}{2} (V_s \Delta t W) \overline{V}_{e_{||}} \delta t,$$

where half the electrons are assumed to be moving away. The current density is, therefore,

$$j = I_e/WL = -\tfrac{1}{2} eN_e \overline{V}_{e||} \sim -\tfrac{1}{4} eN_e \overline{V}_e.$$

From Table 1, its value is 2.4 milliamps/m^2 at Orbiter altitudes. This is the maximum electron current available from the ambient medium since any applied potentials are shielded within a distance H.

The theory for a spherical satellite with a *conducting* skin is well established and confirmed experimentally. To determine the surface equipotential $\emptyset$, the electron current is equated to the ion ram current. If the electron speed distribution is Maxwellian at temperature T_e, the electron current from both directions along the magnetic field onto the circular cross section (πr_s^2) is given by

$$I_e = -2(\pi r_s^2) \left(\tfrac{1}{4} eN_e \overline{V}_e\right) \exp (e\emptyset/kT_e).$$

The ion ram current swept up by the vehicle is

$$I_i = (\pi r_s^2)\, e\, N_i\, \overline{V}_s$$

In the steady state, net charge flow to the satellite must vanish, and, therefore,

$$\emptyset = -\frac{kT_e}{e} \ln (V_e/2V_s)$$

At 400 km, $\emptyset$ = -0.66 volts according to Table 1. A more thorough analysis including ion thermal motion, wake effects, and photoemission at 400 km alters this result only slightly to $\emptyset$ = -0.63 volts.

The foregoing results are not directly applicable to conditions on the Orbiter for several reasons. Since most of the outer surface is a dielectric, it is not an equipotential, and local charging must be computed from expressions for the local current. The Orbiter's complicated shape and variety of attitudes prevents simple solutions as well. However, in the steady state, some useful conclusions can be drawn about local ambient potentials. The following quantitative values are only rough estimates since crude approximations are used.

As an initial basis for estimating the ambient potential at various locations around the Orbiter, the simple Maxwellian theory (Beard and Johnson, 1961) is used. This theory ignores the microscopic effect of the geomagnetic field; collections of local particle current is equally probable in *all* directions. This is reasonably justified because the skin potential is shielded in just a few Debye lengths which is comparable to an electron gyroradius, and local distortion of the particle orbit near the skin does not alter current collection appreciably. Blocking of particle current by the vehicle structure is important, and magnetic shielding affects current collection normal to the field beyond distances of the order of a few gyroradii.

The theory for particle flux in a Maxwellian plasma at local electrical potential $\emptyset$ leads to the following expressions for the current density *toward* the surface due to electrons (Appendix A):

$$j_e = I_e/a = j_{eo} \exp(e\emptyset/kT_e), \quad \emptyset < 0;$$

$$= j_{eo}(1 + e\emptyset/kT_e), \quad \emptyset > 0;$$

and due to ions:

$$j_{iVs} = I_i/a_{\perp Vs} = j_{is}(1 - e\emptyset/\tfrac{1}{2}MV_s^2), \qquad \text{Ram}, \quad e\emptyset < \tfrac{1}{2}MV_s^2;$$

$$j_i = I_i/a = j_{io} \exp\left(-\frac{e\emptyset + \tfrac{1}{2}MV_s^2}{kT_i}\right), \qquad -\tfrac{1}{2}MV_s^2 < e\emptyset < \infty;$$

$$= j_{io}\left(1 + \frac{|e\emptyset| - \tfrac{1}{2}MV_s^2}{kT_i}\right), \qquad e\emptyset < -\tfrac{1}{2}MV_s^2.$$

The constants are defined by

$$j_{eo} = -\tfrac{1}{4}\, eN_\infty \bar{V}_e = -2.4 \times 10^{-3} \text{ amps/m}^2,$$

$$j_{is} = e\, N_\infty\, V_s = +2.6 \times 10^{-4} \text{ amps/m}^2,$$

$$j_{io} = \tfrac{1}{4}\, eN_\infty \bar{V}_i = 1.0 \times 10^{-6} \text{ amps/m}^2,$$

where the particle charge e is always positive and $N_\infty = N_i = N_e$ is the ambient plasma density. The ion ram energy, $\tfrac{1}{2}\, MV_s^2$, is 3.9 eV.

Another source of current *toward* the vehicle is photoemission of electrons by solar ultraviolet, which for most all spacecraft materials is about (Kasha, 1969)

$$j_{ph} = I_{ph}/a'_{\perp sun} = 1.0 \times 10^{-5} \text{ amps/m}^2$$

Its magnitude may fluctuate by a factor of 3, but the foregoing value is assumed to be representative to the same accuracy as the particle flux estimates.

[Thermionic emission of electrons proves to be a negligible source of current for neutralizing the vehicle charge. The theory for metals (Sproull, 1956; Smith, 1958) gives the Richardson - Dushman equation for the current,

$$j_t = AT_s^2 \exp\,(-e\phi_w/kT_s),$$

where $A \simeq 10^6$ amp/m^2 deg^2, T_s is the temperature of the surface, and $e\phi_w$ is the characteristic work function. For the borosilicate coating on the insulating material and for most metals ϕ_w is about 4 volts. Assuming the surface is shaded, T_s is probably ~ 175°K and $kT_s/e \sim 0.015$ volts. The available current is, therefore,

$$\ln j_t \text{ (amps/m}^2) \sim -243$$

which is clearly miniscule. The magnitude of the current varies rapidly with surface temperature but its effect may be ignored here.]

Finally, leakage current through the thermal insulation to the inner metal liner over the superstructure is an important outer skin discharging process under some circumstances. For a potential ϕ_D on the outer skin and ϕ_C on the inner superstructure, the positive current *toward* the skin is

$$j_l = \sigma_i (\phi_C - \phi_D)/\Delta h$$

where σ_i is the electrical conductivity of the thermal insulation and Δh is the insulator thickness. According to Table 2, $\sigma_i \sim 5 \times 10^{-10}$ mhos/m and from Figures 3-5, the thickness varies from 1 to 10 cm. Thus the current is approximately

$$j_l \text{ (amps/m}^2\text{)} \simeq 2 \times 10^{-8} [\phi_C \text{ (volts)} - \phi_D \text{ (volts)}]$$

with a variation amounting to a factor of three.

Some representative examples of ambient skin potentials on the Orbiter may be calculated from the foregoing expressions.

Case A. Leading edges are ram dominated by ion current j_{iVs} and neutralized by j_e which gives an equilibrium potential $\bar{\phi} = -.6$ volt.

Case B. When large areas are shielded from both sunlight and ram ions (e.g., bottomside in ram direction), only electron current reaches the surface from the plasma. The negative potential builds steadily due to electron current from the high-energy Maxwellian tail until equilibrium is established with the insulator leakage current. If it is assumed that the inner structure is at a potential of -0.6 volts due to metal contact with the plasma somewhere else on the vehicle, the local outer skin potential comes to equilibrium at $\bar{\phi}_s = -3.3$ volts.

Case C. Sunlit surfaces that are not accessible to ram ions come to equilibrium with thermal electrons at $\bar{\phi}_s = -1.2$ volts.

Case D. Many non-ram surfaces are accessible to the ion ram current because they are within range of the ion gyroradius. The intensity of the ion current depends on geometry but is expected to diminish linearly with distance from j_{iVs} to J_i. In general, much faster electrons have access to any surface that can be reached by ions. Thus, for non-sunlit surfaces $\overline{\phi}_s$ varies from $\sim$ -0.6 volt to $\sim$ -3.9 volts. However, insulation leakage current limits the lower potential to -3.3 volts according to Case B.

Case E. Due to unusual surface geometry or spacecraft attitude, a few small areas may be accessible to ram ions due to their large gyroradii, but inaccessible to electrons due to their small gyroradii. Typical areas are the exterior surface of the bay door that is shielded from below by the wing, the underside of the tunnel to the spacelab, and possibly under pallet packages. Thus, a net positive charge will build up until steady equilibrium is established. In this case the leakage current through the insulation is negligible and equilibrium occurs at the ram potential $\overline{\phi}_s = \frac{1}{2} MV_s^2 = +3.9$ volts.

A typical operational configuration for the orbiter is shown in Figure 6a and and b to illustrate these specific cases. The foregoing potentials were calculated for steady-state conditions. Since the current of electrons decreases exponentially as the negative potential builds up, it takes a finite amount of time to achieve quasi-equilibrium (within 10% of the final value). However, it can be shown (Appendix B) that the transient time to achieve equilibrium is extremely short, on the order of microseconds. According to the theoretical results, the characteristic e-folding time for the rate-of-change of electron current is $\tau = 4\sqrt{2}\lambda_D / \overline{V}_e = 3 \times 10^{-7}$ seconds using values from Table 1 and 3. An order of magnitude approximation for the time to achieve equilibrium with the electron current is

$$\overline{t} = \tau |e\overline{\phi}_s| / kT$$

For cases A to D, $\overline{t}$ varies from 1 to 5 μ sec. Similarly, for equilibrium with the ion ram current $\overline{t}$ 5 μ sec. This rapid potential buildup is largely attributable to thin Debye shielding of the spacecraft potential which limits the retarding electric field effects to distances of the order

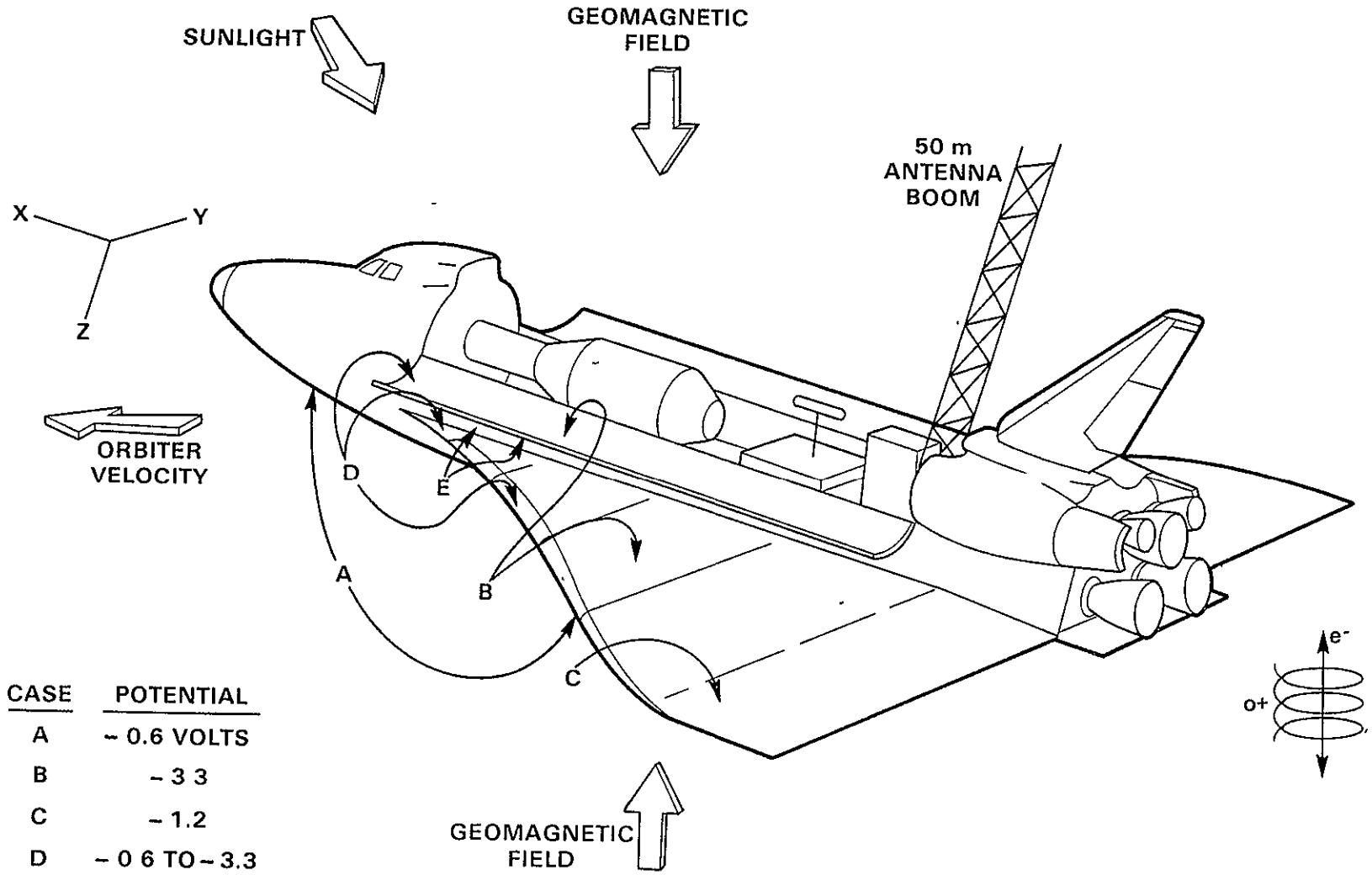

CASE	POTENTIAL
A	~ 0.6 VOLTS
B	– 3 3
C	– 1.2
D	– 0 6 TO – 3.3
E	+ 3.9

FIGURE 6a

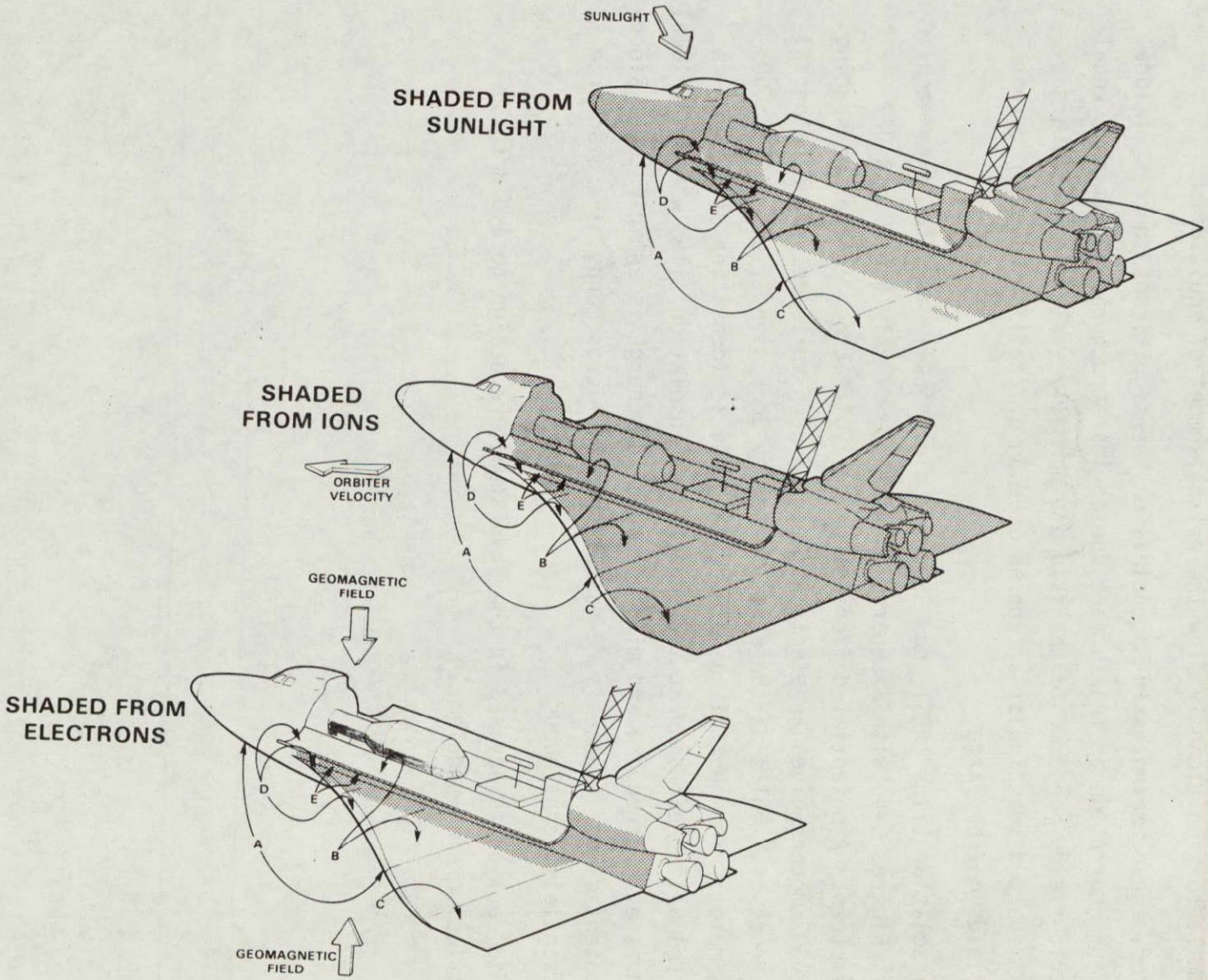
SUNLIGHT
SHADED FROM SUNLIGHT
SHADED FROM IONS
ORBITER VELOCITY
GEOMAGNETIC FIELD
SHADED FROM ELECTRONS
GEOMAGNETIC FIELD
A
B
C
D
E

FIGURE 6b

of a particle gyroradius. The ambient potentials on the skin are simply too small to significantly slow the establishment of equilibrium.

However, these ambient skin potentials may be significant sources of local "battery" corrosion on the surface due to its structural qualities. Local electric fields *parallel* to the skin are normally small over plane areas, but at sharp discontinuities such as leading or trailing edges or corners the fields may be large.

The insulation tiles (HRSI and LRSI) are electrically isolated from each other (Figures 3-4) with a separation distance of only 0.014 to 0.027 centimeters. A potential difference of one volt across an average spacing of 0.0002 meters gives an electric field of 5000 volts/meter. A potential difference of 7 volts at the edge of the bay door gives fields of 35,000 volts/meter. The neutral gas around the vehicle (densities of 2×10^{14} m^{-3} or more) will break down at the edge of the insulation tiles where the local field is even stronger, and minute coronal discharge is anticipated. Since the potential difference is re-established in microseconds, the discharge is essentially continuous.

Remedial action is advised in the skin structure design to avoid this electrical arcing problem.

D. High Potential Induced by Electron Gun

Firing large currents of high-energy electrons away from the AMPS Spacelab produces a net positive charge on the Shuttle orbiter that must be neutralized by return electron current from the plasma surrounding the vehicle. The neutralization process is complicated by several factors which must be considered in its analysis. The large charge involved (on the order of coulombs) may produce large positive vehicle potentials if return currents are inadequate. This potential would result in strong electric fields around the vehicle that can ionize the neutral gas emanating from the vehicle as well as the ambient ionosphere, which increases the available return current. The rapid motion of the orbiter relative to the ions produces a positve charge in the spacecraft wake that affects return current collection. Finally, the dielectric nature of the thermal insulation means that the neutralization current does not efficiently return to the electrical ground of the electron gun; instead it causes differential charging between insulator outer surfaces and the inner metallic superstructure. Evidently, the temporal behavior of these processes is critical for determination of the magnitude of local charging and electric fields. Clearly, it is important to avoid generating potentials that do not allow the beam to escape or that cause electrical breakdown and significant arcing in the thermal insulation.

The theory for satellite potentials induced by large currents of high-energy electrons has been developed for spherical metal vehicles (Beard and Johnson, 1961; Parker and Murphy, 1967; and Linson, 1969). Unfortunately, the theory does not apply directly to the Shuttle-Orbiter configuration, and the theoretical results are not in close agreement with rocket experiments. Furthermore, they are steady-state solutions that describe continuous electron emission rather than current pulses. Nevertheless, they indicate the magnitude of the problem and their results are summarized here.

The theories assume that the background plasma is entirely ionospheric; there is no consideration of satellite sources of gas or additional plasma. Furthermore, the theories ignore additional ionization of the ambient

ionosphere caused by the high electric fields radiating from the vehicle. The return current is assumed to be derived from a Maxwellian distribution of electrons. The differences in the three theories are entirely attributable to the way in which the geomagnetic field affects the electron trajectories. Since the electrons move much faster than the vehicle, the spacecraft is assumed to be stationary and wake effects are ignored. Thus, the equipotential conducting sphere is immersed in a uniform homogeneous plasma and the only anisotropy arises from inclusion of the geomagnetic field. Despite these simplifications, the plasma physics is not trivial, the mathematics is extensive, and the results are qualitative order of magnitude estimates.

Two important parameters are common to all of these theories. One is the return electron current

$$I_o = 2\ (\pi r_s^2)\ j_e$$

where r_s is the radius of the sphere. This form assumes that field-aligned electron current is collected from above and below by the circular cross-section. The other parameter is the potential quantity

$$\phi_o = \frac{m\Omega r_s^2}{2e}$$

where $\Omega = eB/m$ is the electron gyeofrequency. This is attributable to the magnetic forces on the electron that affect the return current collection capability.

In the initial analysis (Beard and Johnson, 1961), the magnetic forces were ignored. For a steady electron emission current I, the potential of the vehicle ϕ is found to be determined by

$$I/I_o = 7\ r_s^{4/7}\ (\phi/\phi_o)^{6/7}$$

Since ϕ rises faster than I, there is evidently a saturation limit where ϕ is sufficient to prevent escape of the electron beam. A subsequent

analysis (Parker and Murphy, 1967) rigorously included the magnetic field effects and obtained the inequality

$$I/I_0 \leq 1 + (4\phi/\phi_0)^{\frac{1}{2}}$$

This form gives much larger potentials for a prescribed beam current due to inhibited collection of return current. Finally, in an effort to bridge the gap between these two theories, a large turbulent region around the vehicle was postulated (Linson, 1969) to increase the collection cross section while retaining the magnetic constraint. This led to the form

$$I/I_0 \sim \frac{2\phi/q_c\phi_0}{\ln(2\phi/q_c\phi_0) - 1}$$

where $q_c = (\omega_p/\omega_c)^2 = N_c\, m/\varepsilon_0 B^2$ is a plasma density parameter in the turbulent region where $N_c >> N_\infty$.

These expressions are displayed in Figure 7 to show their relative shape and magnitude for typical parameter values in the ionosphere. The interesting conclusion is that a 1 m sphere that emits 0.5 amp continuously ($I/I_0 = 10^2$) is predicted to have a potential of 10^4-10^6 volts depending on the theoretical model. Such enormous potentials would inhibit or destroy beams of 10-100 keV electrons. Thus, it is imperative to ascertain the reliability of these predictions.

There have been several rocket experiments which fired electron beams, and the data from these experiments may provide some indication of the vehicle potential. However, because the experiments have successfully launched the beams, there has been little investigation or analysis of data pertaining to the ultimate induced potential of the vehicle. The electron echo experiments (Hendrickson et al., 1971; Winckler, 1974, Winckler, et al., 1975) fired beams upward along the field lines and observed the electromagnetic emissions and electrons after they had echoed back from the other hemisphere. Electron beams from rockets were also fired into the atmosphere to generate artificial auroras (Hess, et al.,

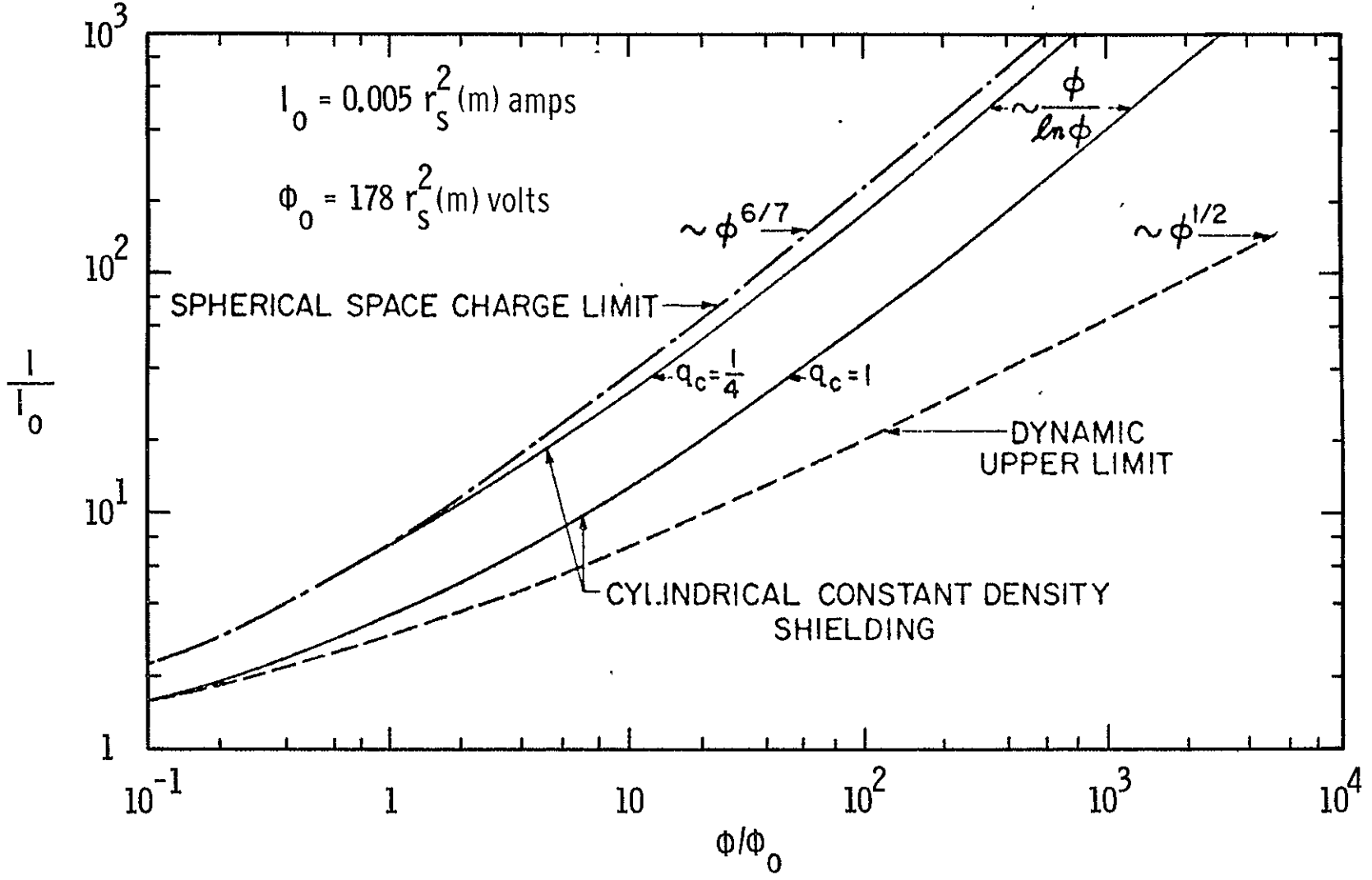
$I_0 = 0.005\ r_s^2$ (m) amps
$\Phi_0 = 178\ r_s^2$ (m) volts
$\sim \phi^{6/7}$
$\sim \frac{\phi}{\ell n \phi}$
$\sim \phi^{1/2}$
SPHERICAL SPACE CHARGE LIMIT
$q_c = \frac{1}{4}$
$q_c = 1$
DYNAMIC UPPER LIMIT
CYLINDRICAL CONSTANT DENSITY SHIELDING
$\frac{I}{I_0}$
Φ/Φ_0
10^3
10^2
10^1
1
10^{-1}
1
10
10^2
10^3
10^4

FIGURE 7

1971). Other rocket experiments involving beam injections into the ionosphere to study excitation processes have also been performed by Air Force Cambridge Research Labs (H. Cohen, private communication).

These electron guns had nominal power levels of a few kilowatts and used accelerator voltages of 1-40 kV. Currents of 5-500 ma were fired in short pulses (10's of milliseconds) at the rate of several times per second. Thus, these experiments are not accurate tests of the foregoing theory, although they do indicate a bound on the voltage excursion. (Evidently, the electron beams were successfully fired away from the rockets, so their potentials must have been limited to something less than a kilovolt.) The return current collection area was just the metal skin of the rocket in most cases (the auroral rocket partially deployed a large conducting "umbrella" to enhance its return current), which is about 10 m^2. Thus, the ambient return current of electrons is perhaps 50 mamps maximum. This is sufficient to balance the gun current in most cases so that large potentials are not expected. Thus, these experiments do not really test the theories properly.

There are special circumstances about the rocket environment that may improve its rapid charge neutralization and maintain the low potentials (H. Cohen, private communication). Offgassing of the rocket motor generates a significant enhancement (orders of magnitude) in the neutral gas density around the vehicle. This atmosphere is partially ionized by those ambient electrons accelerating toward the vehicle potential (100 volts, say). The ionization cross section for electrons is about 5×10^{-18} cm^2 for atmospheric constituents (Brown, 1967, p 141) which necessitates ambient densities of $10^{21} m^{-3}$ for mean free paths of 10 m or less. Each ionizing collision requires about 35 eV of primary energy (Chamberlain, 1961, p 283), so that production is limited to at most two or three pairs per primary. This secondary cascade process has not been observed experimentally, but it does provide a plausible source of additional electrons.

The rocket potential may be measured indirectly by observing changes in the flux of charged particles to the vehicle. Such measurements are

available in a few cases, but the data has not been used to identify the vehicle potential. Local enhancements in the ambient ionization due to surface electric fields might also be discernible in measurements of the return current energy distribution. An experimental study is advocated to establish an empirical model for the generation of local enhanced ionization around the Orbiter.

The Shuttle Orbiter has its own peculiar characteristics that distinguish it from the foregoing rockets or satellites. First, and foremost is its enormous size which provides a return current collection area of 1300 m^2 on dielectric and 60 m^2 on metallic conductor (this metal surface area is almost an order of magnitude more than many rockets). The large dielectric area causes more serious discharging problems since the vehicle is no longer on equipotential as in the all-metal case. Second, the shape of the Orbiter-Spacelab has many sharp corners and edges that produce very high electric fields with only modest potentials. Thus, local ionization enhancements and breakdown arcing are to be anticipated. Third, the neutral atmosphere around the vehicle is well above ambient as indicated in Table 6. Thus, some cascading of electron return current is anticipated during electron gun firing.

When the electron gun is operated the overall potential of the vehicle is driven positive. The thermal electrons in the ionosphere provide a field-aligned return current of up to 2.4 ma/m^2 (Section C). The cross section of surface area available to collect the current varies with vehicle orientation relative to the geomagnetic field. A effective collection area of 1000 m^2 is assumed here (500 m^2 each, above and below). Thus the ambient return current can balance up to 2.4 amps of gun current. Unfortunately the return charge is mostly collected on the dielectric thermal insulation and does not directly neutralize the gun potential.

The electron gun is presumably grounded to the metallic superstructure of the vehicle which has an external surface area of only 60 m^2 or so. Thus, with proper orientation to take full advantage of the conductor cross section, the direct return current to the gun amounts to 150 ma. It is reasonable to conclude that this level of gun current can be accommodated without undue charging of the Orbiter dielectric insulation. For gun currents in excess

of 150 ma, the electric potential is expected to increase significantly, large electric fields are generated, and the dielectric is charged up.

To illustrate some magnitudes, consider a 10 amp gun current pulse for 100 ms which is a coulomb of charge. If the return current is limited to ambient ionospheric background levels, it requires 400 ms for the Orbiter skin to acquire 1 coulomb. Most of the charge is collected on the dielectric insulation and subsequently leaks to the metallic inner structure. The time constant, τ_{RC}, for such current leakage is about 50 ms (overall resistance of 10^5 ohms and capacitance of 0.5 uf). Thus, full discharging requires a significant fraction of a second.

An upper limit on the vehicle potential can be estimated approximately using the theory for an isolated sphere. The surface area of the Shuttle Orbiter is equivalent to a sphere with a 10 m radius. An electrically isolated sphere of this size has a capacitance of 10^{-9} farads. Thus, when it is charged to 1 coulomb, its relative potential is 10^9 volts. Fortunately, the Orbiter is immersed in a plasma that provides return current and suppresses this potential by orders of magnitude. However, even limited surface charging must induce large potentials of the vehicle relative to the plasma.

The effect of large vehicle potentials on the surrounding plasma distribution is uncertain. Some general properties can be surmised, however. If the potential exceeds + 4 volts, the ion ram current is stopped. Since electrons are accelerated to the vehicle, there is a net positive charge in the vehicle wake. Its total charge is probably comparable to the charge in the gun current pulse. Again, consider a 10 amp gun current for 100 ms. In 100 ms the Orbiter has travelled 800 m and its wake diameter is at least comparable to its dimensions, say 50 m. Thus, the volume of the wake charge is at least 1.5×10^6 m^3, and the excess charge density is less than 4×10^{12} ions/m^3. At this level the density is almost comparable to the ambient plasma density (2×10^{11} ions/m^3). Due to coulomb forces and plasma instabilities the charge rapidly dissipates as electron return current enters the wake.

During operation of the electron gun the increase in Orbiter potential is accompanied by large electric fields. These fields are not as sharply

discontinuous as in the ambient situation (Section C), however, and their local magnitude over the dielectric is difficult to estimate. Over sharply curved regions, however, potentials of 100 volts will generate fields of 10^4 volts/m around 1 cm radii. Protruding metal surfaces are apt to be even more sharply curved. These local areas of high electric fields can accelerate ambient electrons and these electrons cause ionization of the neutral atmosphere. Although the process is insignificant over much of the vehicle, there are locations where the neutral density is high (Table 6) and appreciable electron-ion pair production is feasible. A notable case is the fuel cell venting over the trailing edge of the wing. As the vehicle potential increases, ionization off the wing increases and return electron current increases. Presumably at some potential the production and collection of return current just balances the emission current of the gun.

The additional atmosphere around the vehicle is also subject to photoionization by solar ultraviolet. Ion-electron pairs are produced at the rate (Banks and Kockarts, 1973, p. 157) of 10^{-7} (sec^{-1}) N_n ($neutrals/m^3$). Thus, some local enhancement of the plasma density occurs around the vehicle. However, the kinetic forces and geomagnetic trapping do not allow a significant buildup. The normally negative potential adds to the dissipation of electrons and the ions are lost due to vehicle motion. Consequently this process may be ignored, and the local electron density is not appreciably different from its ambient ionospheric level.

A theoretical model for this overall vehicle-plasma interaction during the electron gun operation has not been developed. The spherical metal satellite theories are evidently inadequate, although they suggest rather large potentials are created. Much more research is needed to develop a quantitative model for the plasma distortion around the vehicle. However, some quantitative limits can be deduced from electrical properties of the vehicle skin.

Since the charge on the thermal insulator dielectric does not leak to the inner conductor immediately, negative charge builds up on the dielectric and reduces its potential relative to the conductor. As the overall vehicle

potential returns to the ambient plasma level, the dielectric potential actually goes negative for a short while. During this interval ion-ram current discharges forward areas on the dielectric but not the shielded areas. A qualitative illustration of the potential and charging scenario is displayed in Figure 8. Evidently the vehicle is charge neutral well before the conductor and dielectric are fully discharged by leakage current.

The equivalent electrical circuit for this process can be solved explicitly to get quantitative estimates for potentials and time constants. Initially the return currents to the dielectric I_D and the conductor I_C are assumed constant. This is reasonable for modest potentials that do not ionize or otherwise enhance current collection. The gun current I_G is also constant during the time interval $0 \leq t \leq t_G$. The dielectric skin may be approximated as a high resistance in parallel with a capacitance. The simple electrical circuit and its current flows are shown in Figure 9a. The effective charge on the capacitor is $Q = Q_C - Q_D > 0$ where Q_C is the charge collected by the conductor and Q_D is the charge on the outer skin of the dielectric. The potential across the capacitor, C = 0.5 uf, is

$$\phi = \phi_C - \phi_D = Q/C.$$

The transient behavior of this circuit is described by Kirchoff's rules for electrical networks. The instantaneous leakage current I_L across the resistance $R = 10^5$ ohms, is determined by the voltage drop around the circuit

$$I_L R + Q/C = 0$$

The sum of the currents to the conductor is

$$I_L - I_C + I_G = dQ_C/dt$$

and the corresponding sum to the dielectric is

$$-I_L - I_D = dQ_D/dt$$

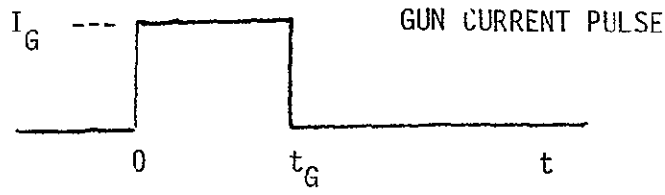
I_G ---
GUN CURRENT PULSE
0
t_G
t

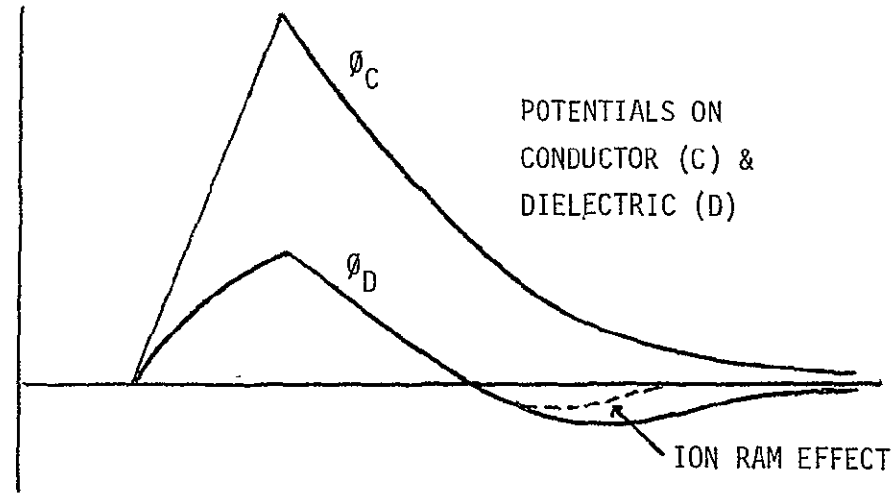
ϕ_C
POTENTIALS ON
CONDUCTOR (C) &
DIELECTRIC (D)
ϕ_D
ION RAM EFFECT

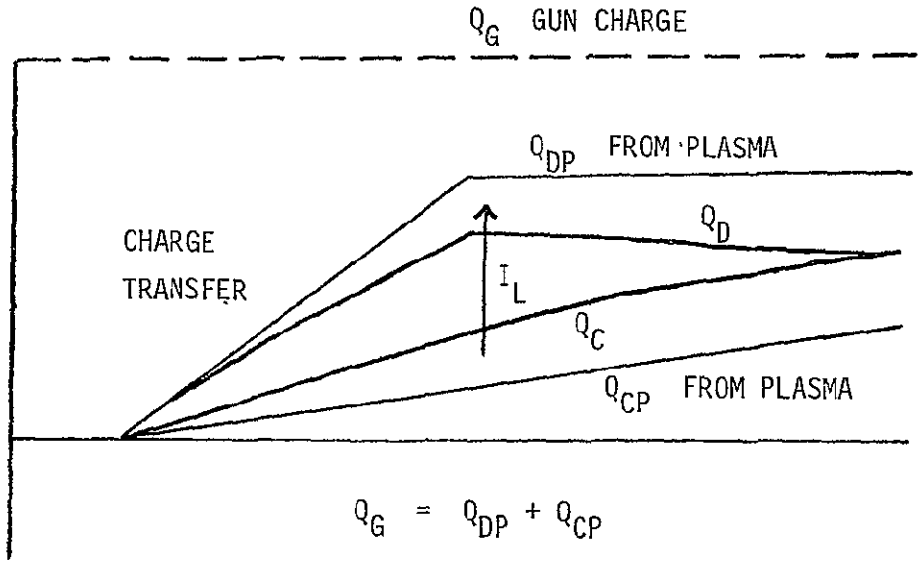
Q_G GUN CHARGE
Q_{DP} FROM PLASMA
Q_D
CHARGE
TRANSFER
I_L
Q_C
Q_{CP} FROM PLASMA
$Q_G = Q_{DP} + Q_{CP}$

FIGURE 8

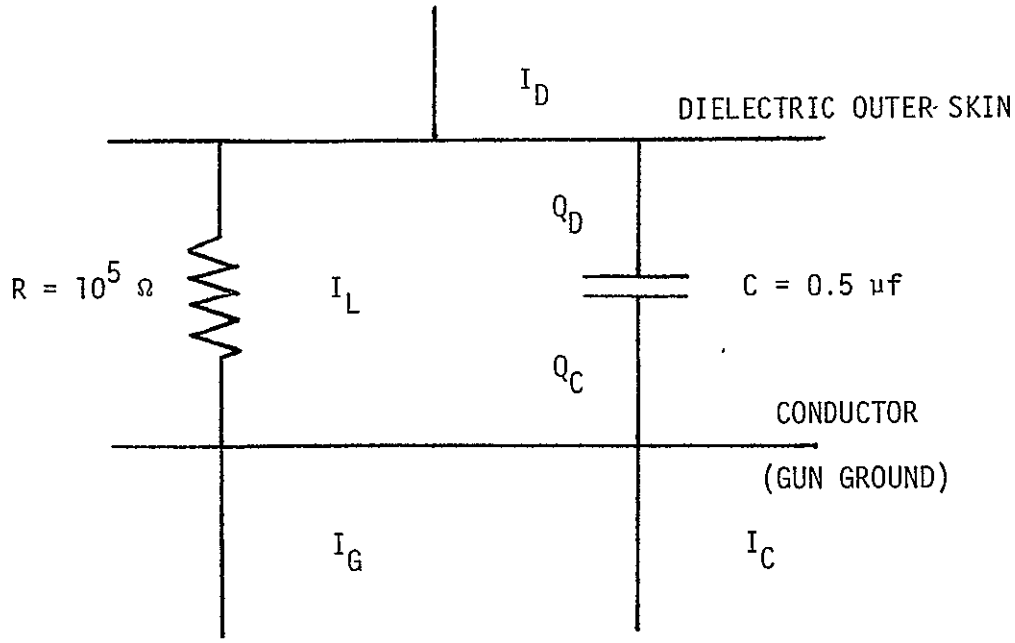
I_D
DIELECTRIC OUTER SKIN
Q_D
$R = 10^5\ \Omega$
I_L
$C = 0.5\ \mu f$
Q_C
CONDUCTOR
(GUN GROUND)
I_G
I_C

(a)

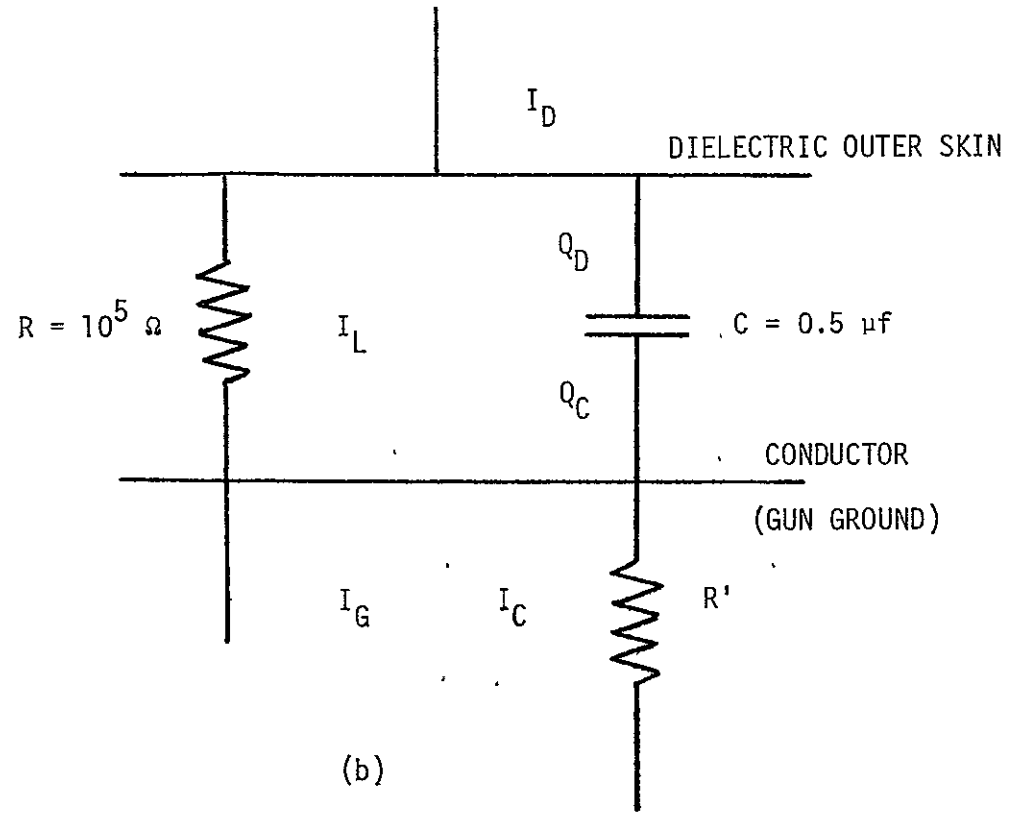
I_D
DIELECTRIC OUTER SKIN
Q_D
$R = 10^5\ \Omega$
I_L
$C = 0.5\ \mu f$
Q_C
CONDUCTOR
(GUN GROUND)
I_G
I_C
R'

(b)

FIGURE 9

Together, these equations specify the temporal behavior of Q and $\emptyset$ across the dielectric.

Subtracting the current equations gives

$$\frac{dQ}{dt} = I_D - I_C + I_G + 2I_L.$$

Eliminating I_L with the voltage equation leads to the elementary differential equation

$$\frac{dQ}{dt} + \frac{2Q}{\tau_{RC}} = I_D - I_C + I_G$$

Its solution has the form

$$Q = \tfrac{1}{2}\,\tau_{RC}\,(I_D - I_C + I_G)\,[1 - \exp(-2t/\tau_{RC})]$$

for $0 \leq t \leq t_G$ and

$$Q = \tfrac{1}{2}\,\tau_{RC}\,(I_D - I_C)\,[1 - \exp\{-2(t-t_G)/\tau_{RC}\}]$$

$$+ Q(t_G)\exp[-2(t-t_G)/\tau_{RC}] \qquad \text{for } t > t_G$$

where $Q(t_G)$ is the maximum charge difference that occurs at $t = t_G$ when the gun current terminates. During the time interval $0 \leq t \leq t_G$, the charge Q increases since $I_G > I_D$, and afterward it decreases.

To test the original assumption that I_C and I_D are constant, consider the illustrative case $I_G = 10$ amps and $t_G = 100$ ms. If $I_D = 2.4$ amps and $I_C = 0.15$ amps, the maximum charge is $Q(t_G) \simeq 0.3$ coulombs. This gives a potential drop across the insulation of

$$\emptyset_C - \emptyset_D = Q(t_G)/C = 600{,}000 \text{ volts}$$

This enormous potential would create electric fields of 24 MV/m across the insulation which is around the electrical breakdown field for good insulators. Thus, the original assumption of moderate potentials is *not* valid, and return current is *not* constant.

Since the conductor is at the higher potential, it is expected to collect more current as $\emptyset$ increases. Thus, as an initial estimate, assume I_C is proportional to $\emptyset$ or

$$I_C = \emptyset/R'$$

where R' is a fictitious plasma resistance that simulates the effect of local ionization and enhanced return current. Its value is unknown, but in general R' < R if $\emptyset$ is to be smaller. Evidently the dielectric insulator potential is not too high so that I_D is assumed to remain constant. The new circuit is shown in Figure 9b.

For these new assumptions, the differential equation for the charge becomes

$$\frac{dQ}{dt} + \frac{2Q}{\tau_{RC}} + \frac{Q}{\tau_{R'C}} = I_D + I_G$$

Thus the same type of solution is obtained with a new time constant

$$\frac{2}{\tau_{RC}} + \frac{1}{\tau_{R'C}} \simeq \frac{1}{\tau_{R'C}} \left(1 + \frac{2\tau_{R'C}}{\tau_{RC}}\right)$$

where it is assumed R' << R. For $t_G >> \tau_{R'C}$, the maximum charge build up across the insulator is reduced to

$$Q(t_G) = \tau_{R'C} \left(1 - \frac{2\tau_{R'C}}{\tau_{RC}}\right) (I_D + I_G)$$

and the corresponding maximum potential is

$$\emptyset_C - \emptyset_D = (I_D + I_G)\, R' \,(1 - 2R'/R)$$

The value of R' seems to be the elusive critical parameter for the process. There is no simple plasma theory for it. A probable range of values may be deduced, however. In order to suppress the induced potential, I_C must grow

to an appreciable fraction of I_G. It is limited by the condition that the total return current cannot exceed the gun current,

$$I_C + I_D \leq I_G$$

In order for the conducting surfaces to collect most of the return current, their potential must be high enough to cause local ionization. This may be achieved with voltages of 10^2 to 10^4 volts to produce electron ionization or electric fields of 10^6 - 10^7 volts/m to produce breakdown in the local atmosphere. Thus, R' is in the range 10^2 - 10^4 ohms. For gun currents of 10 amps the conductor potential is probably 10^3 - 10^5 volts. The time constant for reaching quasi-steady state conditions is 50 μs to 5 ms. Thus the rise time on the potential is extremely short compared to typical gun pulses of 10 ms or more.

In the ambient ionosphere these vehicle potentials probably limit useful gun current pulses to 1 amp or so. Higher beam currents would drive the conductor potential to levels that inhibit the escape of the beam. The induced potentials across the thermal insulation are probably well below the insulator breakdown. However, experimental measurements of electrical properties of the thermal insulation have not been made; they have been surmised from similar materials. As a consequence of the foregoing uncertainties it would be advisable to perform control experiments to establish an empirical behavior pattern.

E. Suppression of Induced Potentials

Other methods have been suggested to aid the collection of return current and suppress the large induced potentials. Presently they are being studied by other investigators and their conclusions about feasibility are not available. Evidently one of these supplementary sources of return current is needed for high gun currents (more than 1 amp).

The most direct method is deployment of a large aluminized balloon on a long tether (P. Banks, UCSD). The balloon provides additional surface area for electron current collection. The long tether generates $\underline{V}_s \times \underline{B}$ electric fields that counteract the induced gun potentials. The magnitude of the available current and potential depends on the size of the balloon and the length of the tether. A few kilowatts appears feasible, but hundreds of kilowatts are needed from this source if it is to be an effective supplement.

Another source of return current is direct ionization of a dense gas cloud by the electron beam of the gun (L. Linson, SAI). If the primary beam interacts strongly with the gas, it can generate an electron cascade of secondaries that contributes to the return current. According to the preceding conclusions (Section D), the electron cascade must be collected by the conductor surfaces, not deposited on the insulator. Fortunately, the large antenna boom can be oriented adjacent to the beam direction. Ionization cross sections and available gas cloud densities limit the efficiency of this process.

Finally, the large VLF antenna offers a conceivable source of return current (R. Benson, NASA Goddard). When this antenna is energized, a sheath of electrons forms along its entire length. The density of the sheath depends on local plasma parameters as well as the driving frequency and power to the antenna.

Hopefully this section can be augmented soon by quantitative estimates for return current collection with these techniques.

APPENDIX A

Ambient Current Calculations

Ambient charged-particle current densities to the Shuttle Orbiter skin may be calculated using elementary kinetic theory when the skin potentials are modest. The basic assumption is that the shielding effects of the plasma restrict the electric field $\underline{E}$ and potential ϕ to a local region adjacent to the skin that is much less than a particle mean free path. The geomagnetic field is assumed to limit the bulk plasma fluid motion to one dimension parallel to the magnetic field $\underline{B}$. However, the velocity space distribution is assumed to be isotropic (Maxwellian), and local distortion at the skin due to $\underline{E}\times\underline{B}$ forces is ignored.

Using these assumptions, the current expressions are developed for a physical model consisting of a circular surface element with radius a at a potential ϕ and a fictitious infinite plane sheet located some distance d above it, where the potential is negligible due to Debye shielding. The objective is to calculate the number of particles passing through the plane sheet that can strike the surface element πa^2. This is a plane-surface analogue of the metallic sphere model (Beard and Johnson, 1961). Its geometry is shown in the accompanying figure.

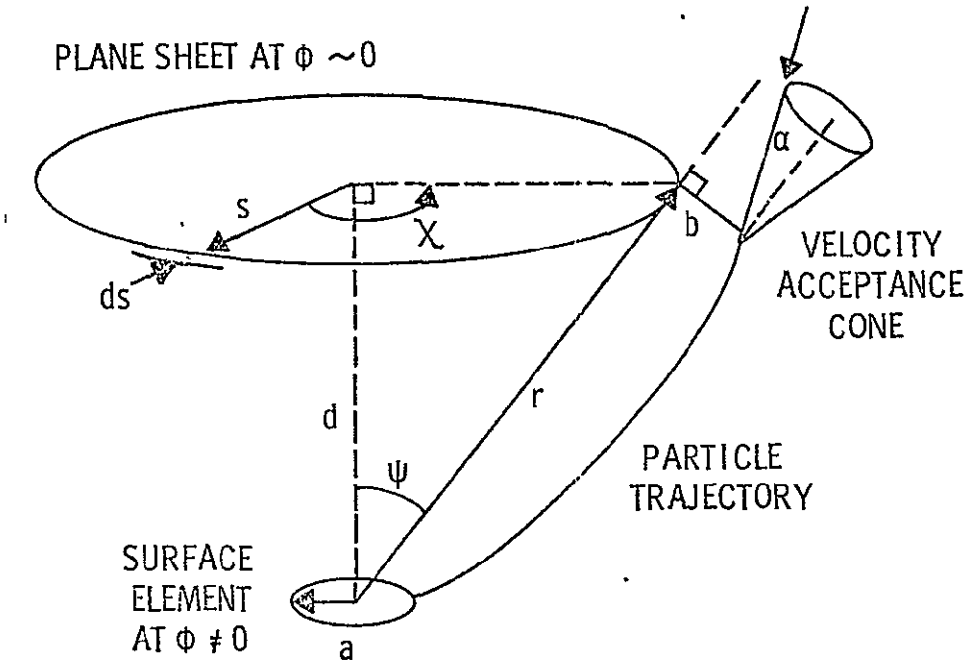

Only a very small fraction of the particle flux through the sheet element s ds $d\chi$ has the proper speed v and direction θ,ϕ to strike any part of the surface element πa^2. They must have velocities that lie inside the cone angle α with respect to the radial direction along r. By geometric considerations

$$\sin \alpha = b/r = b \cos \psi/d$$

where b is the "impact parameter" of the particles normal to the radial direction. By conservation of angular momentum along the trajectory between the sheet and the surface element,

$$mvb = mua \cos \psi,$$

where v is the initial speed in the field-free region beyond the sheet and u is the velocity at impact with the surface. Therefore, from conservation of energy

$$b^2/a^2 \cos^2\psi = (1 - q\phi/\tfrac{1}{2} mv^2)$$

As expected for b = 0, there is a minimum initial speed required to reach the surface:

$$v_o = \sqrt{2e\phi/m} \qquad \text{for } q\phi > 0$$

$$= 0 \qquad \text{for } q\phi < 0$$

Since the particle velocity distribution is Maxwellian in a field-free region, the current of particles traversing the sheet that strike the surface πa^2 is given by the integral

$$I = qN_\infty (m/2\pi kT)^{3/2} \int_0^\infty sds \int_0^{2\pi} d\chi \int_{v_0}^\infty dv \int_0^\alpha d\theta$$

$$\int_0^{2\pi} d\phi \; v^3 \cos\theta \sin\theta \exp(-\tfrac{1}{2} mv^2 kT)$$

Since α is a function of v, the $\theta\phi$ integration is performed first,

$$\int_0^\alpha \int_0^{2\pi} \cos\theta \, d(\cos\theta) \, d\phi = \pi \sin^2\alpha$$

$$= \pi a^2 \cos^4\psi \, (1 - q\phi/\tfrac{1}{2} mv^2)/d^2$$

Subsequent integration over speed v gives

$$\frac{\pi a^2 \cos^4\psi}{d^2} \left(\frac{m}{2\pi kT}\right)^{3/2} \int_{v_0}^\infty dv \; v^3 \left(1 - \frac{q\phi}{\tfrac{1}{2} mv^2}\right) \exp\left(-\frac{\tfrac{1}{2} mv^2}{kT}\right)$$

$$= \frac{a^2 \cos^4\psi}{2d^2} \left(\frac{2kT}{\pi m}\right)^{1/2} \left(1 + \frac{\tfrac{1}{2} mv_0^2}{kT} - \frac{q\phi}{kT}\right) \exp\left(-\frac{\tfrac{1}{2} mv_0^2}{kT}\right)$$

Integration over the sheet is most easily accomplished using the transformation $s = d \tan\psi$, such that

$$\int_0^\infty s \, ds \int_0^{2\pi} d\chi \, \frac{\cos^4\psi}{d^2} = 2\pi \int_0^1 \cos\psi \, d(\cos\psi) = \pi$$

Combining the foregoing integrals gives a current density of the form

$$I/\pi a^2 = \tfrac{1}{4}\, qN_\infty \bar{V} \exp(-q\phi/kT) \qquad q\phi > 0$$

$$= \tfrac{1}{4}\, qN_\infty \bar{V}\, (1 - q\phi/kT) \qquad q\phi < 0$$

where $\bar{V} = (8kT/\pi M)^{\frac{1}{2}}$ is the arithmetic mean (average) speed.

These general expressions for the current density have been used in Section C for the local current density expressions. The electron current j_e is obtained directly by setting $q = -e$ where e is positive. Due to the spacecraft motion V_s, the ions have an apparent directed kinetic energy $\frac{1}{2}\, MV_s^2$ which is not taken into account explicitly by the foregoing theory. Theoretical expressions for j_i are obtained semi-quantitatively for the non-ram situation by including the streaming as an additional ion potential energy relative to the vehicle so that $q\phi \rightarrow + e\phi + \frac{1}{2}\, MV_s^2$.

The expression for the ion ram current contains an additional factor $(1 - e\phi/\frac{1}{2}\, MV_s^2)$ that takes into account local electric field effects (Chang and Smith, 1959).

APPENDIX B

Charging Rate of Orbiter Surfaces

The time dependence of charge buildup on the surface of spacecraft can be determined analytically for simple situations that are good approximations to conditions on the Shuttle Orbiter. Due to the dominant influence of the ambient electron flux, the analysis is initially restricted to electrons alone, and the influence of the ram ion current, photoemission, and insulation leakage current are ignored. Their inclusion would not alter the charging rate appreciably, but the additional terms unduly complicate the analysis. Modifications due to photoemission and ion ram current effects are also illustrated.

Adjacent to a plasma boundary at negative potential ϕ, the electron density is described by

$$N(z,t) = N_\infty \exp\left[e\phi(z,t)/kT\right]$$

where N_∞ is the ambient density at infinity. The instantaneous potential is determined by the Poisson equation

$$\frac{d^2\phi}{dz^2} = \frac{eN_\infty}{\varepsilon_o} \exp(e\phi/kT) + \text{small terms}$$

subject to the condition $\phi = 0$ at infinity. The small terms are ignored, since they do not affect the charging rate appreciably. The solution for ϕ is given implicitly by

$$\frac{\sqrt{2}z}{\lambda_D} = \frac{e\phi}{kT} - \frac{e\phi_s}{kT} + \ln\left|\frac{1-\exp(e\phi_s/kT)}{1-\exp(e\phi/kT)}\right|$$

where $\phi_s = \phi(z=0)$ is the applied surface potential.

The local electric field at the surface is equal to the surface charge,

$$\Sigma = -\varepsilon_o \left[d\phi/dz\right]_{z=0} = -\sqrt{2}\, eN_\infty \lambda_D \left[1 - \exp(e\phi_s/kT)\right]$$

The rate at which Σ is built up with time is just the electron current to the surface

$$j_e\ (z = 0) = -\ \tfrac{1}{4}\ eN_\infty \overline{V}_e\ \exp\ (e\phi_s/kT)$$
$$= d\Sigma/dt = (\ \sqrt{2}\ e^2 N_\infty \lambda_D/kT)\ \exp\ (e\phi_s/kT)(d\phi_s/dt)$$

The time dependence of the surface potential is obtained by integration,

$$\phi_s\ (t) = -(kT/e)\ t/\tau$$

where the characteristic time constant is defined by

$$\tau = 4\sqrt{2}\ \lambda_D/\overline{V}_e$$

The corresponding electron current varies as

$$j_e = j_{eo}\ \exp\ (-t/\tau)$$

These expressions for the time dependence of ϕ_s and j_e describe the initial buildup behavior but do not approach the correct steady state value $\overline{\phi}_s$ due to omission of those small terms that become important near equilibrium. Nevertheless, because $\overline{\phi} >> kT/e$, in general, the expressions are valid for $t >> \tau$, and τ is an acceptable measure of the charging rate. Order of magnitude estimates for the total time to reach equilibrium are simply

$$\overline{t} = \tau|e\ \overline{\phi}_s|/kT$$

Near equilibrium a good approximation is obtained by introducing the other current expressions (j_i, j_{ph}, j_l) as appropriate. For example, including J_{ph}, which is assumed constant leads to the implicit form

$$-t/\tau = e\phi_s/kT + \ln\left|\frac{1 + \dfrac{j_{ph}}{j_{eo}}\ \exp\ (-e\phi_s/kT)}{1 + \dfrac{j_{ph}}{j_{eo}}}\right|$$

As $t \to \infty$, the potential must satisfy $\exp(e\phi_s/kT) = |j_{ph}/j_{eo}|$ as required for Case D. More complicated expressions may be developed for the other cases.

When the ion ram current is the principal source of charge, as in Case E, the Poisson equation for the instantaneous potential $\phi > 0$ has the form

$$\frac{d^2\phi}{dz^2} = \frac{eN_\infty}{t_o} \left(1 - \frac{e\phi}{\tfrac{1}{2}MV_s^2}\right)$$

This may be manipulated to obtain the electric field at the surface

$$-\left[d\phi/dz\right]_{z=0} = \frac{\tfrac{1}{2}MV_s^2}{e\lambda_s} \left[1 - \left(1 - \frac{e\phi_s}{\tfrac{1}{2}MV_s^2}\right)^2\right]^{\frac{1}{2}}$$

where

$$\lambda_s = \left(\frac{\epsilon_o \tfrac{1}{2}MV_s^2}{e^2 N_\infty}\right)^{\frac{1}{2}} = \left(\frac{\tfrac{1}{2}MV_s^2}{kT_e}\right)^{\frac{1}{2}} \lambda_D$$

Equating the charge build up to the ram current gives

$$j_{iVs}\ (z = 0) = eN_\infty V_s \left(1 - e\phi_s/\tfrac{1}{2}MV_s^2\right)$$

$$= d\Sigma/dt = \frac{e\, N_\infty \lambda_s \left(1 - e\phi_s/\tfrac{1}{2}MV_s^2\right)}{\left[1 - \left(1 - e\phi_s/\tfrac{1}{2}MV_s^2\right)^2\right]^{\frac{1}{2}}} \frac{e}{\tfrac{1}{2}MV_s^2} \frac{d\phi_s}{dt}$$

This reduces to the integral

$$t/\tau_s = \int_0^{e\phi_s/\frac{1}{2}MV_s^2} dy \Big/ \left[1 - (1 - y)^2\right]^{\frac{1}{2}} = \frac{\pi}{2} - \sin^{-1}\left(1 - \frac{e\phi_s}{\tfrac{1}{2}MV_s^2}\right)$$

where

$$\tau_s = \lambda_s/V_s = (M/96m)^{\frac{1}{2}} \sim 18\,\tau$$

Since $e\phi_s \quad \tfrac{1}{2}MV_s^2$, an order of magnitude estimate for the time to reach equilibrium is, simply $\bar{t} \sim \tau_s$

REFERENCES

Al'pert, Ya. L., A. V. Gurevich, and L. P. Pitaevskii, Space Physics with Artificial Satellites, translat. H. H. Nickle, Consultants Bureau, New York, 1965.

Banks, P. M., and G. Kockarts, Aeronomy Parts A and B, Academic Press, New York, 1973.

Beard, D. B., and F. S. Johnson, Ionospheric limitations on attainable satellite potential, J. Geophys. Res., 66, 4113-4122, 1961; also Correction, J. Geophys Res., 71, 4707, 1966.

Brown, S. C., Basic Data of Plasma Physics, 1966, MIT Press, Cambridge, 1967.

Chamberlain, J. W., Physics of the Aurora and Airglow, Academic Press, New York, 1961.

Chang, H. H. C., and M. C. Smith, On the drag of a spherical satellite moving in a partially ionized atmosphere, J. Brit. Interplanetary Soc., 17, 199-205, 1959.

Hanson, W. B., Structure of the ionosphere, in Satellite Environment Handbook, 2nd edition, ed. F. S. Johnson, Stanford University Press, Stanford, pp 23-49, 1965.

Hendrickson, R. A., R. W. McEntire, and J. R. Winckler, Electron echo experiment: a new magnetospheric probe, Nature, 230, 564-566, 1971.

Hess, W. N., M. C. Trickel, T. N. Davis, W. C. Beggs, G. E. Kraft, E. Stassinopoulos, and E. J. R. Maier, Artificial aurora experiment: Experiment and principal results, J. Geophys. Res., 76, 6067-6081, 1971.

Johnson, F. S., Structure of the upper atmosphere, in Satellite Environment Handbook, 2nd Edition, ed. F. S. Johnson, Stanford University Press, Stanford, pp. 3-20, 1965.

Kasha, M. A., The Ionosphere and Its Interaction with Satellites, Gordon and Breach, New York, 1969.

Linson, L. M., Current-voltage characteristics of an electron-emitting satellite in the ionosphere, J. Geophys. Res., 74, 2368-2375, 1969.

Parker, L. W., and B. L. Murphy, Potential buildup on an electron-emitting ionospheric satellite, J. Geophys. Res., 72, 1631-1636, 1967.

Rantanen, R. O., and E. B. Ress, Payload/Orbiter Contamination Control Assessment Support, Tech Rpt MCR 75-13 by Martin Marietta Aerospace, for NASA Johnson Space Center NAS 9-14212, June 1975.

Rishbeth, H., and O. K. Garriott, Intro to Ionspheric Physics, Academic Press, New York, 1969.

Smith, L. P., Thumionic Emission, in Handbook of Physics, eds. E. U. Condon and H. Odishaw, McGraw-Hill, New York, pp 8-74 to 8-82, 1958.

Sproull, R. L., Modern Physics, Wiley, New York, sec. 12-2, 1956.

Whitten, R. C., and I. G. Poppoff, Fundamentals of Aeronomy, Wiley, New York, 1971.

Winckler, J. R., R. L. Arnoldy, and R. A. Hendrickson, Echo 2: A study of electron beams injected into the high-latitude ionosphere from a large sounding rocket, J. Geophys. Res., 80, 2083-2088, 1975.

Winckler, J. R., Investigation of electron dynamics in the magnetosphere with electron beams injected from sounding rockets, J. Geophys. 40, 729-749, 1974.

SPACECRAFT PAYLOAD OPTIMIZATION

by

H. B. Liemohn, W. A. Reardon and R. L. Engel

BATTELLE
Pacific Northwest Laboratories
Richland, Washington 99352

June 1975

For Presentation to
NASA/MSFC Shuttle Spacelab Working Group on
Atmospheric, Magnetospheric, and Plasmas-in-Space

Submitted for Publication in
Trans. American Geophysical Union

SPACECRAFT PAYLOAD OPTIMIZATION

by

H. B. Liemohn, W. A. Reardon and R. L. Engel

ABSTRACT

Many factors are considered in the selection and integration of scientific experiments for spacecraft payloads. Ideally, the payload should provide maximum scientific value subject to the finite limitations of cost, telemetry, power, weight and volume imposed by the scope of the mission. Operations Research offers a useful tool for selection of experiment options where several payload parameters are constrained. Each proposed experiment is defined by a set of options corresponding to successively higher levels of sophistication and scientific value. Experimental parameters for each option are presumed to be specified by the proposer, whereas the scientific value of each option is determined by a review process that may ignore the other factors. Selection of experiment options that simultaneously maximize scientific value and satisfy constraint limits on the payload is achieved by conventional integer programming. Payload integration requirements may also be included by additional side conditions which enhance scientific value for certain combinations of experimental options. Of course, other subjective considerations are also important in the selection of payloads, but this proposed method provides a useful quantitative guideline.

INTRODUCTION

The selection of spacecraft payloads is frequently a source of consternation for proposers of experiments as well as mission administrators. Large amounts of money and maintenance of technical staffs as well as personal prestige and scientific careers are at stake in these deliberations. The unique nature of spacecraft experiments requires very specialized knowledge for the review process which is usually only available from principal investigators of previous spacecraft experiments. Owing to the limited opportunities for missions, a small group of capable experimenters has emerged.

We are now embarking on a new era of space science research. With the advent of the Space Shuttle for near Earth research there will be ample opportunity for a much wider range of experiments. In addition to studies of the atmosphere and magnetosphere environment, it is anticipated that the Shuttle will also carry a variety of experiments devoted to astronomy, materials processing, bio-medical investigations, other commercial applications in communications and earth resource evaluation, and expanded applications of a military nature. There will also be many new opportunities for participation on Deep-Space Probes to study the Moon, Sun, other Planets, and interplanetary debris.

These expanded opportunities are accompanied by certain complications. NASA budget limitations will place severe constraints on the expenditures for individual experiments. There will be strong encouragement for new

institutions to participate in the space program which includes new inexperienced personnel. This will be partially offset in the Shuttle program by the Spacelab concept, wherein basic instruments are designed for repetitive usage in a variety of experimental objectives. The long duration of interplanetary missions demands a long-term commitment on the part of principal investigators, from experimental conception to data interpretation.

In this new era of broader mission objectives, much wider participation in spacecraft experiments is desirable. In such circumstances, the selection of experiments is anticipated to become much more difficult due to a variety of factors. First, the community of potential spacecraft experimenters has expanded enormously through our educational system. Second, much more diverse payload opportunities are expected to attract new areas of research which heretofore had not considered spacecraft laboratories for their investigations. Third, constraining conditions on individual payloads are apt to become much more elaborate as the experiments grow larger and more complex. Thus, some systematic way of quantifying part of the experiment selection process might be appropriate at this time.

METHOD

The methods of operations research have been applied to many multiparameter decision situations and its application to spacecraft payloads appears to be feasible as well. The only new concept introduced here is parametric modelling of experiment options, a step that is frequently taken implicitly in the course of developing experiments but rarely used explicitly

to evaluate them. Once the experimental options have been parameterized, all the proposed experiments must be graded quantitatively according to their relative scientific value; a method for making such judgments is suggested below. Most importantly, this value judgment can be based on scientific merit alone, independent of other nonscientific factors. Once this parameter array for the experiment options is defined, a straightforward application of integer programming techniques yields a selection of experiments for optimum usage of the total payload profile.

A given spacecraft mission is usually subject to five basic constraints. First, there is a limitation on the total cost of the mission which usually limits the total cost of all experiments. Second, the data obtained by the instruments must be telemetered to available receivers on the ground over a limited radio bandwidth which specifies the rate at which information can be transmitted. Third, the total power available to operate the experiment is limited by the generating capacity of the solar panels, radioisotope thermoelectric sources or other devices. Fourth, the launch vehicle capability and the mission trajectory define the permissible payload weight. Finally, the volume of the payload is restricted by the launch vehicle configuration.

Thus, for each experiment option we must define a cost, C, a telemetry bandwidth, T, a power requirement, P, a weight, W, and a volume, V. Selection of a set of experiment options is subject to the following constraint inequalities:

$$0 \leq CT = \Sigma C \leq CT_m \quad (1)$$

$$0 \leq TM = \Sigma T \leq TM_m \quad (2)$$

$$0 \leq PW = \Sigma P \leq PW_m \quad (3)$$

$$0 \leq WT = \Sigma W \leq WT_m \quad (4)$$

$$0 \leq VM = \Sigma V \leq VM_m \quad (5)$$

where CT_m, TM_m, PW_m, WT_m, and VM_m are maximum limits on the consumption.

Establishing a scientific value for each experiment option, S, relative to all others is indeed difficult particularly with diverse experiments. Nevertheless, it has been done repeatedly by payload selection committees, and it should be easier to quantify when other constraints can be ignored. As a practical matter, a group of experts might grade the options individually and then average their recommendations to obtain a concensus on each option. This technique is sometimes called the Delphi method after its origin as described in Appendix A. The ultimate objective, of course, is to *maximize* the scientific value

$$SV = \Sigma S \quad (6)$$

for a prescribed group of options.

Finding the maximum of (6) subject to conditions (1) - (5) is the province of linear programming.[1] It consists of a rigorous mathematical procedure for examining various option combinations in the hyperspace of experiment parameters subject to the linear constraint conditions. Integer programming[2] is mandatory since fractions of an experiment option are meaningless. The optimization process is illustrated by a simple analytic example in Appendix B.

While the mathematical procedure for linear programming is rigorous, the answer is not always unique. Sometimes more than one location in the hyperspace (combinations of options) will yield the same maximum scientific value and still satisfy the constraint conditions. Another important consideration is the fact that incremental changes in the constraint conditions can significantly alter the selection of options and the ultimate maximum scientific value. This is particularly true for integer programming where a particular option combination may lie on the border line of the constraint condition. Thus, a small group of possible combinations might be more appropriately identified depending on the rigidity of the constraint conditions.

This optimization technique for payload selection provides an opportunity to perform variational studies under "what if" conditions. For example, the addition of another power source might decrease the weight and volume available for the payload but would increase the available power and thereby modify the constraint conditions and change the option combinations. A change in the trajectory or speed on a distant planetary mission might significantly relax the weight requirement and allow additional experiments. In the course of building the experiments that have been selected, there are frequently changes in individual operating parameters such as power, weight or volume as well as revisions in cost estimates, and these changes occasionally lead to a reassessment of the optimum configuration. Finally, certain experiments are considered to be a mandatory part of the payload for housekeeping data, background levels, or perhaps public relations, and it might be interesting to ascertain the minimum scientific value needed to insure their inclusion.

The integration of payload experiments frequently imposes coupling conditions on two or more experiments. In many experimental studies the background noise for one experiment is the desired signal in another experiment. Similarly, small expansions of one experiment may add significantly to the scientific value of many others. Thus, when one experiment is selected, certain other experiments are more attractive. This concept can be incorporated into the linear programming method by introducing coupled options with enhanced scientific value.

Duplication of experiments is another factor in payload selection. In some instances redundancy is a desirable precaution against loss of vital measurements. In other cases, duplication would be wasteful of spacecraft resources and should be avoided. These alternative conditions in the selection process can be introduced by appropriate auxiliary constraints.

EXAMPLE

In order to illustrate the method, experiment options have been modeled for a deep-space scientific research payload to another planet. The detailed option information is presented in Table 1 for seven experiments that might be considered for such a mission. The numerical entries are entirely arbitrary and are not based on any experimental design criteria. The seven proposed experiments consist of a television camera, a life sciences experiment, cosmic ray detectors, various plasma probes, a broadband radio receiver, a radio frequency sounder, and a mass spectrometer.

The options within each experiment are fairly apparent from their descriptive titles. Some comments are appropriate, however, to explain the variations in the tabular entries. For example, the basic television camera is expected to have a reasonably high scientific value and a high telemetry rate. The addition of a data processor eliminates much of the redundant data, sharply reducing the telemetry requirements but possibly losing some fine structure detail and thereby reducing its overall scientific value slightly. A two or three color camera is undoubtedly much more valuable but without the data processor its telemetry requirements are enormous. Finally, an onboard recorder for multiple picture data storage is considered the ultimate option because it eliminates much of the telemetry congestion .

The life sciences experiment runs through a series of sampling techniques from an onboard sensor, through a subsatellite, to some type of lander device. Although no provision has been made to allow more than one option

TABLE 1

DEEP-SPACE SCIENTIFIC RESEARCH PAYLOAD
MODEL OF EXPERIMENT OPTIONS

Option Description	Option Number	Scientific Value	Cost 10^6\$	Telemetry kbps	Power Watts	Weight kgms	Volume $10^3 cm^3$
		TV - TELEVISION CAMERA/IMAGE PROCESSOR					
Basic Camera	1	5	8	20	15	20	2
Data Processor	2	4	10	10	16	21	2.1
Two-color Camera	3	8	12	35	18	28	2.5
Data Processor	4	7	13	18	19	30	2.6
Three-color Camera	5	12	14	50	21	33	3.0
Data Processor	6	10	15	24	21	34	3.0
Picture Recorder	7	14	20	30	21	36	2.6
		LS - LIFE SCIENCES/AMINO ACIDS, BACTERIA					
Air Sampler	1	4	3	2	7	13	3
Sophisticated Processing	2	6	5	5	8	14	3
Subsatellite	3	7	8	4	9	15	3.3
Low-altitude Sampler	4	10	10	3	10	17	2.5
Lander	5	15	15	6	14	22	4.5
		CR - COSMIC RAYS/GEIGER TUBES, SCINTILLATORS					
Geiger Tubes	1	0.5	0.2	0.5	1	2	1.0
Telescope Coincidence	2	1.5	0.7	2.0	6	5	3.0
Scintillators	3	3.0	1.3	4.0	5	4	2.5
Computer Processing	4	5.0	1.7	3.0	7	5	4
Sophisticated Array	5	7.0	2.0	5.0	8	5	4

Option Description	Option Number	Scientific Value	Cost 10^6 $	Telemetry kbps	Power Watts	Weight kgms	Volume 10^3 cm^3
PP - PLASMA PROBE/LANGMUIR PROBE, FARADAY CUP							
Langmuir Probe	1	1.0	1.2	1.0	4	1	0.5
Faraday Cup	2	1.5	1.4	2.0	5	1.5	0.5
Computer Processing	3	3.0	1.7	1.0	8	3.5	1.5
Improved Sensitivity	4	4.0	1.8	2.0	8	3.5	1.6
Sophisticated Array	5	5.0	2.0	3.0	10	4.0	1.8
RR - RADIO RECEIVER/ULF, ELF, VLF, LF							
Limited Band LF	1	0.5	0.3	0.5	5	10	0.5
Broadband VLF-LF	2	1.5	0.4	5.0	4	10	0.5
Ultra Broadband ULF-LF	3	4.0	0.5	15.0	7	12	0.5
Computer Processing VLF-LF	4	2.0	0.8	2.5	10	17	1.5
Computer Processing ULF-LF	5	3.0	1.0	3.0	11	18	1.5
Record/Playback	6	5.0	2.0	2.0	14	20	2.0
RS - RADIO SOUNDER/LF, MF, HF							
Discrete Sounder MF	1	2.0	0.7	3.0	13	20	1.5
Discrete Sounder LF-HF	2	3.5	0.9	6.0	14	20	1.5
Computer Process LF-HF	3	2.5	1.3	2.0	16	24	1.9
Full Ionosonde LF-HF	4	4.5	1.4	4.0	16	24	1.9
Record Only	5	7.0	1.6	3.0	19	29	2.3
Compute/Record	6	8.0	2.0	2.5	21	30	2.5
MS - MASS SPECTROMETER/LOW Z - MED Z							
Selected Masses	1	1	1	2	3	1	0.7
Swept Mass-Low Z	2	2	1.5	4	4	1.2	0.8
Computer Process-Low Z	3	3.5	2.0	5	4	1.3	0.8
Computer Process-All Z	4	5.0	3.5	8	6	2.0	1.3

in each experiment, it would be possible in life sciences, for example, to combine two or more preceeding options into an additional option for consideration.

The other five experiments that are proposed here have been flown numerous times on various spacecraft using various levels of sophistication. Although hard data might be available for the tabular entries of these experiment options, they have not been used here. The tabular entries were made up by the authors for purely illustrative purposes and do not describe any particular experiment.

The optimum payload selection for nine different constraint conditions is displayed in Table 2. The cost is allowed to increase steadily whereas the other constraint parameters are incremented at intervals much as the constraints on a real spacecraft. The constraint maxima were determined in advance and not altered to fit any special requirement. It is notable that the parameter summations are usually near their maximum limit; in other words, the option selection shifts to most fully utilize the available facilities.

Cases I, V, VI, VII and VIII exhibit multiple solutions. This is most likely an artifact of the simple integer nature of the constraints. In all cases the second solution is obtained by substituting one or two experiments with a small change in one or more of the constraint variables. The cases V and VI are interesting in that each has two solutions and those of Case V are identical to those of Case VI. The only constraint relaxed between Cases V and VI was the allowable cost but apparently not enough to allow a new experiment to enter the solution.

TABLE 2

SPACECRAFT PAYLOAD
SCIENTIFIC RESEARCH OPTIMIZATION

CASE	I		II	III	IV	V	
	CR5	CR5	LS1	LS4	LS4	LS5	LS5
PAYLOAD	RR5	PP5	CR5	CR5	CR5	CR	CR5
SELECTION	M53	M53	RR5	M53	PP5	PP4	PP5
			MS4		RR6	RR6	RR3
					MS4	MS4	MS4
Scientific Value SV	13.5	13.5	17.5	20.5	32.0	36.0	36.0
Cost $\frac{CT}{CT_m}$	4.4/5	4.4/5	8.9/10	14/15	19.5/20	24.3/25	23/25
Telemetry $\frac{TM}{TM_m}$	13/20	17.4/20	(20/20)	13/20	21/40	23/40	37/40
Power $\frac{PW}{PW_m}$	22/25	22/25	(25/25)	22/25	48/50	(50/50)	45/50
Weight $\frac{WT}{WT_m}$	19/30	19/30	(30/30)	23.3/30	48/60	52.5/60	45/60
Volume $\frac{VM}{VM_m}$	6.3/10	6.3/10	8 8/10	7.3/10	11.6/15	13.4/15	12.1/15

CASE	VI		VII		VIII		IX
	LS5	LS5	LS5	LS5	TV6	TV3	TV7
PAYLOAD	CR5	CR5	TV3	TV3	LS5	LS5	LS5
SELECTION	PP4	PP5	CR5	CR5	CR5	CR5	CR5
	RR6	RR3	PP4	PP5	PP5	PP5	PP5
	MS4	MS4	RS6	RS5	RS6	RS5	RR6
			MS3	MS3	MS4	MS4	MS4
Scientific Value SV	36.0	36.0	45.5	45.5	47.0	47.0	51.0
Cost $\frac{CT}{CT_m}$	24.3/30	23.0/30	34.8/35	34.6/35	39.5/40	36.1/40	44.5/45
Telemetry $\frac{TM}{TM_m}$	23/40	37/40	55.5/60	57.0/60	48/60	(60/60)	54/60
Power $\frac{PW}{PW_m}$	(50/50)	45/50	73/75	73/75	73/75	(75/75)	73/75
Weight $\frac{WT}{WT_m}$	52.5/60	45.0/60	89.8/90	89.3/90	87/90	(90/90)	89/90
Volume $\frac{VM}{VM_m}$	13.4/15	12 1/15	15.9/20	15.9/20	16.6/20	16.4/20	16.2/20

The existence of multiple solutions (or even the enumeration of feasible nearby solutions) would enhance the use of the Delphi technique by providing an input to a second round of expert concensus. A good deal more information is available from the computer output. The limiting constraints are identified; in Table 2 the circled quantities indicate such constraints. When no constraint is indicated as limiting there is a little of everything left over which might provide some useful design information for altering an experiment or designing an additional experiment to fill the gap. The tool described can provide the basis of iteration between the program managers and the scientific community.

CONCLUSION

In conclusion it must be emphasized that this proposed method is merely an aid to optimization of spacecraft payloads which must be augmented by prudent judgment. Application of the method clearly displays the relative importance of the constraint boundaries and demonstrates where they may be relaxed or tightened without affecting the overall mission objectives. Evidence suggests that the selection process tends to fill the spacecraft to capacity in all the constraint variables.

Utilization of this operations research method would significantly streamline the administration of payload selection. Individual proposers would be requested to identify their set of options with appropriate parameters and brief descriptions of the capability within each option. On the basis of the capability statements the scientific value could be established by a small group of impartial experts. If the option data were programmed in advance, the selection process could be performed with a direct computer link in real time. This would provide the committee with the opportunity to vary constraints and scientific value estimates to determine a cluster of option combinations. Such quantitative output should speed up the decision process by eliminating many qualitative side issues.

Hopefully, this method can be tested in the selection of a real payload sometime soon.

Appendix A. The Delphi Technique

There are many advantages and disadvantages to a committee of experts, some of which are:

Advantages	Disadvantages
More information available	More misinformation available
Errors can be corrected	Strong social pressures bias the committee behavior
Committees will take more chances	Number of arguments rather than validity tends to carry the day
	Rearching agreement may become more important than accuracy
	Strong personalities tend to dominate
	"Winning" may tend to freeze arguments
	Committee shares a common bias

In an effort to preserve the advantages and obviate the disadvantages a method (or series of methods) of consulting the Oracles has been developed called the Delphi method[3]. It's principal features are, anonymity, iteration with controlled feedback and statistical group response. More specifically these features accomplish the following:

(a) anonymity - The group members are not known to each thus obviating social pressures, dominance, "winning", etc. An idea should be tried on its merits only and minds may change with no loss of face or esteem.

(b) Iteration with Controlled Feedback - The group iteration is carried out via questionnaires, thus only relevant information need be extracted from the responses and fedback for reconsideration. The respondent is only informed of the current status of the collective opinion, both majority and minority. The group does not take on a separate identity and goals.

(c) Statistical Group Response - Committees commonly turn out a majority opinion and perhaps a minority report. The Delphi response may include the whole spectrum of response presented in any of several common statistical measures: mean, standard deviation, quartile groups, etc.

The iteration may be continued through as many rounds as the interrogating group or manager feels useful. There have been many applications and variations of the technique carried out and reported in the literature of operations research and management science.

An excellent discussion of the method, details of procedures, do's and don'ts, and references are available[4].

Appendix B. Linear Programming

The method can perhaps be illuminated with a simple example. Let us assume the following problem:

$$\begin{aligned} \text{Maximize:} \quad & X_1 + 2X_2 = Z \\ \text{Subject to:} \quad & X_1 + X_2 \leq 6 \\ & -X_1 + 3X_2 \leq 10 \\ & X_1 - X_2 \leq 2 \\ & (X_1, X_2) \geq 0 \end{aligned}$$

The set of constraints is shown in Figure 1. For simplicity the constraints are shown as equations and the arrows indicate the direction which the inequality would require. Clearly the lines (including the axes) define a closed region in which each point represents a feasible set (X_1, X_2) satisfying all the constraints. The feasible integer sets are set out by the dots. The solution to the problem is indicated by the dashed line:

$$X_1 + 2X_2 = 10, \quad X_1 = 2, \; X_2 = 4.$$

This set represents the largest value of Z which satisfies all the constraints. The line for Z = 11 is also shown to show that it lies outside the feasible region. Clearly if the slope of the function Z were different it would be possible to have more than one integer solution to the problem, in which case the solution is said to be degenerate. Various algorithms exist to solve these kinds of problems, which get very complicated as the number of equations and variables increase.

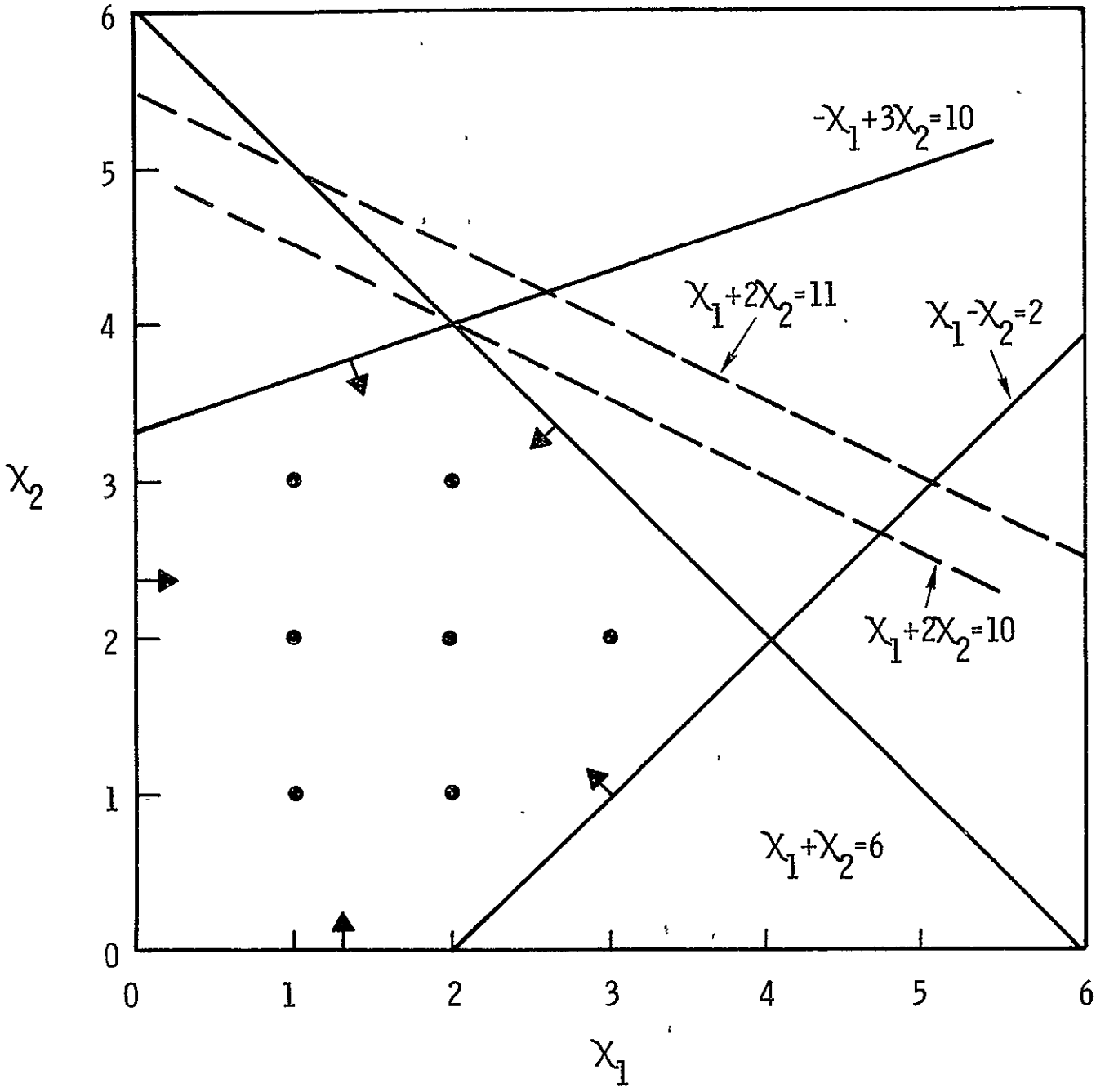

FIGURE 1

REFERENCES

1. See, for example, Dantzig, George B., Linear Programming and Extensions, Princeton University Press, 1963.
2. See, for example, Hu, T. C., Integer Programming and Network Flows, Addison-Wesley, 1969.
3. Dalkey, N., "The Delphi Method, An Experimental Study of Group Reaction," Rand Memorandum RM-5888-PR, The Rand Corporation, Santa Monica, CA, 1969.
4. See, for example, Martino, J. P., Technological Forecasting for Decision Making, Elsevier, New York, 1972.

Hydromagnetic Wave Measurements

Objectives:

Natural hydromagnetic waves (0.01 to 10 hZ) propagate throughout the ionosphere and magnetosphere, and their characteristic frequency-time signatures provide a useful measure of dynamic plasma processes in the medium. The Space Shuttle offers the opportunity to systematically study propagation within the ionospheric waveguide (100 to 1000 km), and assess the hydromagnetic energy transmission between the magnetosphere where it is presumably generated, and ground stations where it is routinely monitored.

A secondary objective is the measurement of field variations caused by ionospheric current systems, anomalies in the terrestrial field, and the local ULF electromagnetic interference around the spacecraft.

Technique:

For the frequency band of interest and anticipated signal-to-noise ratios, the best instrumentation appears to be triaxial fluxgate magnetometers. Owing to the large EMI on the spacecraft, the measurements must be performed on a subsatellite that is inertially stabilized. Fluxgate magnetometers, which measure the instantaneous vector components of the local magnetic field, are well established satellite research instruments.

Detection of hydromagnetic waves requires a local EMI below 3×10^{-7} gauss rms which makes subsatellite operation mandatory. Due to the low altitude and high speed (~0.1 wave phase velocity), effects of local ionospheric currents and ground magnetic anomalies place severe requirements on signal processing. In order to sort out such secondary effects,

an array of subsatellites equipped with magnetometers would be desirable. Systematic comparison of satellite and ground network measurements is clearly essential to differentiate local properties.

Requirements:

Although the fluxgate principle is well known and used extensively, further instrument development is essential to achieve the desired sensitivity to natural wave amplitudes that are 10^{-6} of the geomagnetic background. On a spinning subsatellite, development of demodulation algorithms will also be required. The fields along the Shuttle orbit limit the useful bandwidth to 0.01 to 10 Hz.

Real-time display of power spectra from each field component from each subsatellite would be desirable. Overlays would provide estimates of instrument reliability and phase relationships that would be useful for the instrument specialist on board the Spacelab. Wave propagation vectors and polarization over a broad range of narrow frequency bands would provide important diagnostics of other active experiments that alter the local medium.

AMPS EXPERIMENT OPERATIONAL REQUIREMENTS (EOR)

1 TITLE	DATE
Hydromagnetic Waves	September 1975
	PREPARED BY. Harold B. Liemohn

2 OBJECTIVE. The measurement of geomagnetic disturbances in the ULF band (0.01 to 10 Hz) with triaxial fluxgate magnetometers on *subsatellites* launched from the AMPS Spacelab.

Natural hydromagnetic waves propagate throughout the ionosphere and magnetosphere, and their characteristic frequency-time signatures provide a useful measure of dynamic plasma processes in the medium. Quasi-steady state magnetic perturbations such as those produced by ionospheric current systems or ground anomalies are also amenable for study from Spacelab altitudes because their transient appearance along the satellite trajectory will generate magnetic disturbances in the frequency band of the detector. Manmade injections of waves, particle beams, or gas clouds may also generate magnetic purturbations that provide measureable diagnostics at hydromagnetic frequencies. Several specific scientific objectives have been identified:

a. Wave Propagation in the Ionosphere Waveguide. The phase velocity at hydromagnetic frequencies has steep gradients above (~1000 km) and below (~100 km) the ionosphere, which provide a unique horizontal waveguide for ULF signals (such as Pc-1). Magnetospheric signals that are guided along geomagnetic field lines enter this waveguide and part of the energy spreads horizontally through mode coupling. The energy slowly dissipates through leakage to the ground and plasma heating. Sensitive triaxial fluxgate magnetometers on one or more subsatellites launched by the AMPS Spacelab would provide important measurements of the horizontal propagation. Close collaboration and coordination with other satellite observations and ground stations is mandatory.

b. Birkeland Current System. The magnetic disturbances associated with polar substorms and magnetic bays are thought to be caused by particle current systems in the ionosphere which were first suggested by Birkeland. Traversal of such current systems at satellite speeds will produce magnetic perturbations with time scales on the order of ULF periods (100 km is traversed in about 14 seconds). The three-dimensional structure and dynamics of these and other ionospheric currents are best surveyed by an array of subsatellites due to the short time scale of events, but close collaboration between an array of ground stations and a single satellite for many events would be adequate.

c. Crustal Anomalies in the Geomagnetic Field. Mapping of the small scale crustal anomalies is a potential byproduct of magnetometer measurements by low-altitude satellites. Motion over such anomalies limits the useful detection of hydromagnetic waves to periods shorter than about 50 seconds. However, measurements for an extended time (months) would permit isolation of the larger anomalies and extend the frequency band for useful wave detection. (An example of "noise" is one application providing the "signal" for another application.)

d. Manmade Wave Generation. Many injection experiments contemplated for the AMPS Spacelab may generate waves at hydromagnetic frequencies. Among them are the pulsed emission of beams of protons and electrons, generation of large-scale conductivity anomalies as with metallic chaff or readily ionizable gas, and artificial magnetic anomalies such as a superconducting dipole. In each case, any hydromagnetic wave energy from these sources might provide useful diagnostic information.

e. Ambient Background Monitor. The local electromagnetic interference (EMI) generated by power equipment and electronics instrumentation on the Shuttle Orbiter includes the ULF band, which prohibits useful magnetic measurements from the AMPS pallet or boom. Magnetic measurements from subsatellites can map the near-field around the vehicle which may affect the integrity of certain experiment sensors. Other experiments involving injections of particles or waves may be affected by the ambient ULF wave fields so that background data is important.

3 INSTRUMENTS. List by name the AMPS instruments required to support the experiment, the function(s) performed by each instrument and the experiment peculiar control functions and displays required

INSTRUMENTS REQUIRED: (Use IFRD title)	INSTRUMENT FUNCTIONS.	CONTROLS AND DISPLAYS.
Triaxial Fluxgate - Located on Subsatellites AMPS IFRD 15	Continuous measurement of the vector magnetic field at a minimum sampling rate of 20 times per second for each component.	Control over 2-3 preselected sampling rates Control of on-board microprocessor functions and its corresponding output format Display power spectra of each component from each subsatellite by colored overlays on one CRT. Display wave propagation vector and/or wave polarization over broad range of narrow frequency bands by colored overlays on one CRT.

ORBITAL CONDITIONS. (Time of year, day, night, altitude, inclination, vehicle attitude, etc.)	TARGET CONDITIONS (Describe location—lat., long.,— size, altitude, etc.)	CREW ACTIVITIES:	4 EXPERIMENT CONDITIONS For each of the experiment conditions, identify the necessary conditions or events which must occur to support the experiment. Present graphically, if possible, on attached sheets
Continuous operation independent of season, diurnal condition, altitude, or inclination. Subsatellite position should be known to within a few kilometers. Vehicle attitude (pitch, roll, and yaw) are required to within 0.5° The spacecraft spin rate must be as slow as possible: optimum - 1 rev/100 sec; tolerable - .1 rev/10 sec; intolerable - 10 revs/sec.	No special target conditions. Collaboration with other satellite magnetometer observations and arrays of ground stations requires accurate position information only. Support of other active or passive experiments on AMPS may require special positioning of the subsatellite.	Periodic (daily) check of instrument readouts to assure proper operation. Possible changes in sampling rate or data format during magnetic disturbances. Possible preparation of subsatellite location or instrument operation in support of other special experiments.	

5 REMARKS.

List other constraints that might be useful in scheduling, support systems sizing, etc.

Due to low altitude and high speed, effects of local ionospheric currents and crustal magnetic anomalies place severe requirements on signal processing. This aspect of the experiment needs further study and evaluation.

Spin demodulation development cost varies as the spin rate since hydromagnetic wave amplitudes of 50 milligamma (0.5×10^{-6} gauss) must be measured against a background geomagnetic field of 0.5 gauss. Thus, a dynamic range of $\pm 10^6$ is required which is slightly beyond the current state-of-the-art.

Signal levels of interest also impose a limit of 30 milligamma (0.3×10^{-6} gauss) RMS on the background EMI of the subsatellite.

AMPS INSTURMENT FUNCTIONAL REQUIREMENTS

PART I — **TECHNICAL INFORMATION** — H. B. Liemohn

1 TITLE Triaxial Fluxgate (Subsatellites) ...

DATE PREPARED 2/4/75

2 OBJECTIVE

Primarily to study natural hydromagnetic wave propagation in the ionosphere waveguide. Secondarily to probe ULF noise generated by Shuttle orbiter and possibly controlled discharges from long tether on ULF antenna.

3. DESCRIPTION (Outline operational modes, briefly describe equipment. Include sketch and/or block diagrams, showing required interfaces with other systems, whenever possible, as an attachment to this form.)

Triaxial fluxgates are well established satellite research instruments. They measure the instantaneous vector components of the local magnetic field. For this mission they are the best method for measuring hydromagnetic waves at frequencies below 0.1 Hz and amplitudes above 5×10^{-7} Gauss (50 m γ). The instrument can only operate efficiently in EMI below 3×10^{-7} Gauss (30 m γ) rms, so that subsatellite operation appears mandatory. Further instrument development is essential to achieve desired sensitivity to natural wave amplitudes that are 10^{-6} of the geomagnetic background that varies at the satellite spin rate.

PART II — **ENGINEERING INFORMATION**

1. WEIGHT, SIZE, AND LOCATION (Give estimated weight, size and location of completed experimental hardware, including unique cabling, plumbing, and support structure.)

EQUIPMENT ITEM	WEIGHT	VOLUME (m^3) STORED	VOLUME (m^3) OPERATION	DIMENSIONS (m) STORED	DIMENSIONS (m) OPERATION	LOCATION EG PRESS, MODULE, PALLET, SUBSAT, ETC
Subsystem 1 Subsystem 2 Subsystem 3 Etc	less than 2 kg	0.001	m^3	About 0.1 x 0.1 x0.1	m	Subsatellite only (2 m boom)
TOTAL						

2 **POWER** (Provide requirements to be supplied by S/C for each subsystem or component in Item 1 above If power consumption not constant state requirements in enough detail so power profiles can be determined Indicate if there are any special requirements for power or voltage to be provided by the instrument

TOTAL S/C POWER REQUIRED (W)	Standby Continuous		4 watts Average	Maximum
	VOLTAGE/POWER REQUIRED BY SEPARATE ASSEMBLIES			
	Voltage (V)	Power (W)	Power (W)	Power (W)
Subsystem # 1	Standard Satellite	Standby Negligible	Average 4 watts	Maximum
Subsystem # 2	Operation	Standby	Average	Maximum
Subsystem # 3	(24 V DC)	Standby	Average	Maximum

3 **DATA MEASUREMENT REQUIREMENTS** (State expected data and measurement characteristics in format specified below where applicable Include additional or different information as necessary)

SCIENCE OR HOUSEKEEPING PARAMETERS TO BE MEASURED	TYPE (DIGITAL ANALOG)	BAND WIDTH OR FREQ RANGE (LOW TO HIGH, Hz)	AMPLITUDE (e g , 0-5 V)	ACCURACY OR WORD LENGTH	MEASMTS PER UNIT TIME OR NO OF CHANNELS	SAMPLING OR BIT RATE
Subsystem # 1 Name Parameter 1 Bx Parameter 2 By Parameter 3 Bz Parameter 4	Digit From Each Subsatellite			Up to 16 bits	1	600 BPS MAX
Subsystem # 2 Parameter 1 Sensor Temp Parameter 2 Electronics Temp Parameter 3 Parameter 4	Analog	Sampled by Subcommutated Analog Channel	0-5B		1/min or less	
Subsystem # 3 Parameter 1 Parameter 2 Parameter 3 Parameter 4						

4 SPACECRAFT ORIENTATION REQUIREMENTS (Outline spacecraft attitude control requirements, pointing accuracy and stability tolerances below)

A Spacecraft pointing accuracy (pitch, roll, yaw) Not required

B Allowable spacecraft rate (pitch, roll, yaw) As slow as possible: Optimum - IREV/1000 sec
Tolerable - IREV/10 sec
Intolerable - 10 REV/S

C S/C attitude knowledge req 0.5°
(pitch, roll, yaw)

D Orbital parameters required for effective instrument operation (explain)
Accurate position

E Instrument operation period To few kilometers
Continuous

F Standby period
Possibly within 1 km of Shuttle if EMI is high

5 CONTROL REQUIREMENTS (Describe those needed by function)

On - Off Command
2 - 3 Sampling Rates
Possible on-board microprocessing and corresponding change in Data bit format

6. DISPLAY REQUIREMENTS

Overlay display of power spectra of each subsatellite component.

Wave propagation vector and polarization display over broad range of narrow frequency bands.

7. INSTRUMENT DEVELOPMENT INFORMATION (If available)

	COST	SCHEDULE
INSTRUMENT PRELIM DESIGN	$0.5 M (Est)	76-77
INSTRUMENT FINAL DESIGN, FABRICATION AND TESTING	0.5 M (Est)	78-79

8. REMARKS (Additional comments on EMI, thermal and Contamination requirements and other support systems, etc.)

Due to low altitude and high speed, effects of local ionosphere currents and ground magnetic anomalies place severe requirements on signal processing. Spin demodulation development cost varies as spin rate due to 0.5 gauss geomagnetic field that requires dynamic range of $\pm 10^{+6}$. Also require background EMI on subsatellite to be less than 3×10^{-7} gauss (30 m γ) RMS.

A Fluxgate Magnetometer for Low Altitude Shuttle Orbit

Interim Report

January 9, 1976

by

Professor Robert L. McPherron
Department of Geophysics and Space Physics
University of California
Los Angeles, California 90024

Consultant's Report
Submitted to:

Dr. H.B. Liemohn
Battelle, Pacific Northwest Laboratories

Introduction

During the 1980's, Space Shuttle will provide a number of opportunities to probe the near earth environment. One of these opportunities is the AMPS Program. The AMPS program is specifically designed to utilize the space shuttle to carry out in situ measurements in the upper ionosphere. Both active and passive experiments are planned as well as arrays of subsatellites and coordinated ground observations.

One important parameter which must be measured during many ionospheric experiments is the earth's magnetic field. At low altitude this field is quite inhomogeneous as a consequence of magnetic materials in the earth's crust and high order terms in the spherical harmonic expansion of the main field. Accurate measurements of the vector magnetic field are needed, for example, to point particle beam accelerators.

Superimposed on the earth's main field are magnetic perturbations due to a number of sources. The largest such perturbations are due to field aligned currents and localized ionospheric currents. The equatorial electrojet and the auroral electrojet are examples of such currents. Initial shuttle missions will probably have near equatorial orbits making studies of the equatorial electrojet quite feasible. Later missions will have orbits of sufficiently high inclination that they will intersect the auroral oval making studies of field-aligned currents and the auroral electrojet possible as well.

Still another, although much smaller, perturbation of the earth's field is the consequence of natural Ultra Low Frequency (ULF) hydromagnetic waves. These waves originate far out in the earth's magnetic field and propagate to the earth's surface. Some of these waves have sufficiently short wavelengths that they become trapped in the low velocity channel created by the peak in electron density of the ionospheric F layer. These waves propagate long distances from their source, parallel to the earth's surface.

One important experiment which will almost certainly be attempted on space shuttle is the artificial generation of ULF waves. Because the wavelength of ULF waves is long compared to those normally used in radio communication they are able to penetrate conductors to much greater depth. This is particularly important in naval communication with submarines which must place antennas above the ocean's surface at the present time. In order to ascertain the success of any attempts to generate ULF waves it will be necessary to continuously monitor the nearby magnetic field.

The space shuttle vehicle as presently planned will not be magnetically clean. With such a large multipurpose vehicle it would be impossible to reduce the spacecraft DC or AC magnetic fields to a sufficiently low level that magnetic measurements of the type described above will not be possible on shuttle itself. Consequently, such measurements will need to be performed on small subsatellites. We note, however, that such spacecraft fields may seriously interfere with other experiments on space shuttle itself. It may in fact be necessary to use a magnetic field on a subsatellite to map and

monitor the shuttle magnetic field in order to properly interpret the results of experiments.

The foregoing discussion enumerates the major reasons for measuring magnetic fields on space shuttle. In abbreviated form, the objectives of this experiment are therefore:

1. Make absolute measurements of the earth's vector magnetic field.

2. Measure magnetic perturbations due to field aligned and ionospheric currents.

3. Observe natural ULF waves propagating in the ionospheric waveguide.

4. Monitor artificial ULF waves generated by shuttle experiments.

5. Monitor the DC and AC magnetic field of space shuttle itself.

These objectives have been previously summarized by H. Liemohn, September, 1975, in the AMPS experiment operational requirements for the hydromagnetic wave sensor. This document suggests that these objectives can be met by a triaxial fluxgate magnetometer on a shuttle subsatellite. It is the purpose of this report to examine the feasibility of using such an instrument. In the body of this report we will examine the constraints imposed on the instrument by these scientific objectives. We will summarize these constraints as a series of instrument specifications. Then we examine the operational principles and performance of modern fluxgates. Finally, we suggest a possible fluxgate design which meets a number of the requirements. We conclude with a discussion of further developments

that must be carried out to fully achieve the stated objectives.

Feasibility of Using a Fluxgate Magnetometer

The feasibility of using fluxgate magnetometers to meet the stated objectives has been adequately demonstrated in situations other than shuttle orbit. As we will show later, the difficulties of low altitude satellite measurements such as these proposed for shuttle are a consequence of rapid motion through the earth's magnetic field and rapid temperature variations.

To demonstrate the capabilities of present fluxgate magnetometers we present a few examples. First, fluxgates can be designed to operate in high fields. Acuna and Ness, 1975, have reported a design capable of measuring the 10 gauss (10^6 gamma) field of Jupiter on the space probe Pioneer 10. Andersen, 1974, has reported the use of fluxgates to continuously monitor the earth's surface magnetic field at automatic magnetic observatories. Rostoker and Kisabeth 1973, have used similar automatic instruments to monitor the magnetic perturbations of the auroral electrojet. This same equipment has been used to monitor ULF waves, Sampson et al., 1971 and Olson and Rostoker, 1975. Similar measurements have been made at lower magnetic latitudes by Lanzerotti, et al., 1971.

Satellite observations of both the main field and ULF waves have been described by several research groups. For example, the synchronous spacecraft ATS 1 and ATS 6 frequently observe the entire spectrum of ULF waves with fluxgate magnetometers, McPherron et al., 1972, 1975. ULF waves have also been observed on eccentric spacecraft McPherron and Coleman, 1971 and Kivelson et al., 1975. At

shuttle altitudes Armstrong and Zmuda, 1973, have measured magnetic perturbations of field aligned currents.

A detailed examination of the various instruments presented in the body of this report shows that no existing fluxgate magnetometer could presently meet all of the objectives outlined above. The reason is easy to understand. Accurate measurements of ULF waves require a resolution of at least 1/16 gamma while measurement of the earth's main field requires a dynamic range of $\pm$ 65,536γ. In other words, the resolution of the measurement must be

$$\frac{1/16}{2(65,536)} = \frac{2^{-4}}{2^{17}} = \frac{1}{2^{21}} = 10^{-6.32}$$

Or about one part in a million. For comparison, the limits of modern analog to digital converters are presently $1/2^{16}$.

Despite this fact, it has been possible to construct fluxgate magnetometers with a resolution of $1/2^{22}$. For example, the UCLA fluxgate magnetometers on OGO-5 and ATS-6 and also in the Air Force Cambridge Magnetic Observatory Network, Snare and Benjamin, 1966; McPherron et al., 1975; Power, 1973, all have this capability. The principle on which these operate is the offset field generator Snare and Spellman, 1967.

An offset field generator is simply a stable source of current which flows through a coil wound around a fluxgate magnetometer sensor. Each time the basic magnetometer goes offscale a discrete amount of current is added or subtracted from this offset coil bringing the magnetometer back to mid-range. The absolute accuracy of the magnetometer is primarily due to the accuracy with which this current can be measured and the constancy of the geometrical

properties of the sensor relative to the offset coil.

The reason such instruments can simultaneously monitor hydromagnetic waves is that the basic magnetometer is scaled so that it is possible to digitize its entire dynamic range with the desired resolution using existing analog to digital converters. Typical scalings are 1/16 gamma in $\pm$ 64γ or 1/2^{11}.

Measurements of this resolution are meaningful only because of the peculiar spectrum of the noise generated by constant current sources. In general it is found that the noise spectrum of the offset field produced by this current has a 1/f frequency dependence. This means that on a long time scale the offset current will drift altering the readout of the basic magnetometer. Thus, while the measurements are precise, they are not accurate. On short time scale, however, the drifts of the offset current are smaller making it possible to measure the small fluctuations associated with ULF waves of comparable time scale.

From the above discussion it would appear feasible to use a fluxgate magnetometer to attain the objectives of the shuttle experiment. Unfortunately, existing magnetometers could not do this. The problem results from magnetometer and telemetry bandwidth constraints. Motion through the earth's magnetic field causes rapid changes in the measured field. For an inertially stabilized spacecraft the rate of change of field is about 100 gamma per second. For a spinning spacecraft with 1 second spin period, the rate is $\approx$300,000 gamma/second. No existing fluxgate magnetometer has a frequency bandwidth sufficiently broad that it

could follow the steps of the offset field generator in this latter case. As we will show in a final section of this report, we believe it is possible to modify existing fluxgate magnetometer designs in such a way that it would be possible to measure the earth's main field with the desired resolution ($\simeq 1/2^{20}$), on a slowly spinning satellite.

The final problem which must be considered in deciding the feasibility of the fluxgate magnetometer is whether the instrument can be made sufficiently accurate to measure the earth's main field for modelling purposes. As we show in the body of this report, the needed absolute accuracy in each field component is of the order 30γ. In a 50,000γ field this is an accuracy of .06%.

Absolute accuracy is a function of several factors. It depends on the location of the spacecraft, the altitude of the spacecraft, the orthogonality of the sensors, and long term drifts in each sensor. From previous experience with total field measurements on POGO spacecraft, Cain and Langel, 1968, it appears that location can probably be determined with sufficient accuracy. However, with respect to spacecraft attitude it is unclear that this is the case. At the pole errors transverse to the main field are approximately

$$\delta B = 60{,}000\gamma \cdot \Delta\theta(\text{radians})$$

for $\delta B \leq 30$ we require $\Delta\theta \leq .029$ degrees or about 1.8 minutes of arc.

Undoubtably, sophisticated star sensors can achieve this accuracy after sufficient data analysis. However, it must be recognized that these measurements must be performed at the location of the magnetometer sensor. This must be at the end of a long

boom which will vibrate and flex as the spacecraft changes attitude and is illuminated, by the sun at different angles. To design equipment capable of such measurements will clearly require considerably engineering effort.

It must be noted that this degree of angular stability must also be present in the fluxgate sensor array as well. While this seems to be possible using large Helmholz coils in temperature controlled rooms on the earth's surface it is much more difficult in satellite sensors. Current satellite sensors do not seem adequate, although appropriate mechanical and thermal design may make such sensors possible.

Another problem is long term drifts in fluxgate sensors. It has been found that drifts in fluxgate readings tend to be proportional to temperature and external field and to change over long intervals of time, Primdahl and Darken, 1971. It appears that this is also a problem of mechanical and thermal design. These causes are probably a consequence of changes in the fluxgate core with respect to surrounding coils.

In summary, it would appear possible to use the offset field generator type of fluxgate magnetometer to meet the objectives of the AMPS mission on the shuttle spacecraft. This design must be modified electronically if the instrument is to operate on a spin stabilized spacecraft. To make absolute measurements of the field, particular attention must be paid to appropriate mechanical and thermal design of the fluxgate sensor array if it is to remain accurate over long intervals of time and large temperature ranges.

Considerable development is also required to determine the attitude of the sensor array at the end of its boom.

References

Acuna, M.H. and N.E. Ness, The Pioneer XI high field fluxgate magnetometer, Space Sci. Instru., 1, 177-188, 1975.

Andersen, F., An automatic magnetic observatory system, Publications of the Earth Physics Branch, Department of Mines and Resources, 44(11), Ottawa, Canada, 1974.

Armstrong, J.C. and A.J. Zmuda, Three axis magnetic measurements and field aligned currents at 800 km in the auroral region: initial results, preprint, Johns Hopkins University, Applied Physics Laboratory, March 1973.

Cain, J.C. and R.A. Langel, The geomagnetic survey by the polar orbiting geophysical observatories OGO-2 and OGO-4 1965-1967, Goddard Space Flight Center, Greenbelt, Md., December 1968.

Lanzerotti, L.J., A.P. Lie and N.A. Tartaglia, Conjugate geomagnetic studies near the plasma pause, Antarctic Journal of the U.S., VI(4) 129, 1971.

McPherron, R.L., and P.J. Coleman, Jr., Satellite observations of band-limited micropulsations during a magnetospheric substorm, JGR, 76(13) 3010, 1971.

McPherron, R.L., P.J. Coleman, Jr., and R.C. Snare, The UCLA fluxgate magnetometer on ATS-6, UCLA IGPP #1482-84, 1975.

McPherron, R.L., C.T. Russell and P.J. Coleman, Jr., Fluctuating magnetic fields in the magnetosphere, Space Sci. Rev., 13, 411-454, 1972.

Olson, J.V. and G. Rostoker, Pi 2 pulsations and the auroral electrojet, Planet. Space Sci., 23, 1129-1139, 1975.

Power, J.J., A digital offset fluxgate magnetometer for use in remote geomagnetic observatories, Scientific Report No. 1, 20, Sept., 1973.

Primdahl, F. and W.R. Darker, Long term stability of a ferrite core fluxgate magnetometer in high field, Geophysical papers, R-25.

Rostoker, G. and J.L. Kisabeth, Response of the polar electrojets in the evening sector to polar magnetic substorms, JGR, 78(25) 5559, 1973.

Samson, J.C., J.A. Jacobs and G. Rostoker, Latitude-dependent characteristics of long period geomagnetic micropulsations, JGR, 76(16), 3675, 1971.

Snare, R.C. and C.R. Benjamin, A magnetic field instrument for the OGO-E spacecraft, IEEE Trans. Nuc. Sci., NS-13(6), 333, Dec. 1966.

Snare, R.C. and Spellman, G.N., Digital offset field generator for spacecraft magnetometers. No. 618, August 28-30, 1967.

Sounding of Shuttle Wake and of Natural Ionospheric Irregularities by Bistatic Doppler Tracking

Objectives:

The wake produced by an orbiting body moving through the ionosphere contains important diagnostic signatures about the spacecraft environment. This disturbance contains in fact information on the unperturbed medium and also provides means of investigating the electrodynamic/aerodynamic properties of bodies of various shapes moving at orbital velocities in an unbounded magnetoplasma. Furthermore, the wake may constitute a potential target for radar diagnostics.

Natural perturbations of the ionospheric electron densities are of comparable relevance. They are: field-aligned columns of enhanced ionization, traveling ionospheric disturbances, ionospheric turbulence, etc.

Techniques:

Repetitive probing of the Shuttle wake in several directions and up to distances where the medium is undisturbed will be carried out between the Shuttle and a subsatellite. The two frequencies (harmonically related) must be phase coherent. Due to plasma dispersity, the electron density distribution in the wake affects the phase velocity of the two waves in a characteristic way. By inverting these phase changes measured at any point of the subsatellite's trajectory, local values of the electron density along the propagation path through the wake can be deduced.

Faraday rotation between the two link's terminals provides the measurement of the total columnar electron content along the radio path. The same link, with the subsatellite connected to a longer tether or free-flying can also be used to measure the natural ionospheric density

perturbations.

Requirements:

This experiment requires a dual-frequency UHF terminal onboard AMPS (162 and 324 MHz could be a suitable pair) equipped with 0.1 watt transmitters, phase-locked receivers, clock and Doppler processor. Similar instrumentation is required on the tethered subsatellite. Ground-based stations could be added to provide further data on the effect of ionospheric perturbations on space-to-earth links within the horizon of each site. Implementations of this instrumentation concept have been worked out for different types of space research (for example, redshift experimentation and measurement of gravity field anomalies). The required differential phase stability (1 part in 10^{15} for 1 second integration time) is within the present state-of-the-art. Weight of the equipment at each terminal (exclusive of 10 km tether) is a few kilograms; size is of the order of 1/100 cubic meter. Power required from AMPS is about 100 watts.

Harold Liemohn
Mario Grossi

AMPS INSTURMENT FUNCTIONAL REQUIREMENTS

PART I — **TECHNICAL INFORMATION**

1 TITLE Doppler-tracking Bistatic Sounder of STS/AMPS Wake — **DATE PREPARED**

2 OBJECTIVE

To measure by the doppler tracking method the electron density distribution in the STS/AMPS wake.
To measure the wake profile up to a distance of 10 Km, in the spherical space around the vehicle.

3 DESCRIPTION (Outline operational modes briefly describe equipment Include sketch and/or block diagrams showing required interfaces with other systems whenever possible, as an attachment to this form.)

A multifrequency doppler link able of measuring differential doppler and rotating (Faraday) doppler is estblished between a tethered satellite (tether length up to 10 Km) and AMPS. The link measures the columnar electron content at various distances from STS , from which a full 3-dimensional model of the wake electron density can be constructed.
The system includes the following subsystems:
Subsystem 1 - 10 Km tether complete with reeling/unreeling mechanism,equiped with sensors to track the position of the free end of the tether.
Subsystem 2 - Satellite connected at the free end of the tether, complete with multifrequency phase-coherent transponder and linear polarization antenna.
Subsystem 3 - AMPS-borne inverted transponder to function as master terminal of the bistatic, multifrequency, phase-coherent sounding link, equiped with linearly polarized antenna.

PART II — **ENGINEERING INFORMATION**

1 WEIGHT, SIZE, AND LOCATION (Give estimated weight, size and location of completed experimental hardware, including unique cabling, plumbing, and support structure.)

EQUIPMENT ITEM	WEIGHT	VOLUME (m^3)		DIMENSIONS (m)		LOCATION EG PRESS, MODULE, PALLET, SUBSAT, ETC
		STORED	OPERATION	STORED	OPERATION	
Subsystem 1	15 Kg	0.01				Pallet
Subsystem 2	20	0.015				Satellite
Subsystem 3	10	0.005				Press.
Etc						
TOTAL	45	0.03				

2 **POWER** (Provide requirements to be supplied by S/C for each subsystem or component in Item 1 above. If power consumption not constant, state requirements in enough detail so power profiles can be determined. Indicate if there are any special requirements for power or voltage to be provided by the instrument

TOTAL S/C POWER REQUIRED (W)	Standby 14 W		Average 85	195 Maximum
	VOLTAGE/POWER REQUIRED BY SEPARATE ASSEMBLIES			
	Voltage (V)	Power (W)	Power (W)	Power (W)
Subsystem # 1	28 V DC 110 V, 400 Hz	Standby 10 W ?	Average 75 W 5	Maximum 150 W 25
Subsystem # 2	Satellite equiped with its own primary power system. Power drain is:	Standby 1	Average 2.5	Maximum 10
Subsystem # 3	110 V, 400 Hz	Standby ?	Average 5	Maximum 20

3 **DATA MEASUREMENT REQUIREMENTS** (State expected data and measurement characteristics in format specified below where applicable. Include additional or different information as necessary.)

SCIENCE OR HOUSEKEEPING PARAMETERS TO BE MEASURED	TYPE (DIGITAL ANALOG)	BAND WIDTH OR FREQ RANGE (LOW TO HIGH, Hz)	AMPLITUDE (e.g., 0-5 V)	ACCURACY OR WORD LENGTH	MEASMTS PER UNIT TIME OR NO. OF CHANNELS	SAMPLING OR BIT RATE
Subsystem # 1 Name						
Parameter 1 tether tension	A	DC to 10 Hz		7	1	10^{-1}
Parameter 2 Range of tether's end	A	DC to 100		17	1	1
Parameter 3 Azimuth	A	DC to 100		10	1	1
Parameter 4 Elevation	A	DC to 100		10	1	1
Subsystem # 2						
Parameter 1 Satellite Temperature	A	DC to 0.1		12	1	10^{-1}
Parameter 2 Battery Voltage/ Current	A	DC		7	2	10^{-2}
Parameter 3 Phase-lock Indication	A	DC to 10		1	3	10^{-1}
Parameter 4 AGC/Tx out. power	A	DC to 10		8	6	10^{-2}
Subsystem # 1						
Parameter 1 AGC	A	DC to 10		8	3	10^{-2}
Parameter 2 Tx output power	A	DC to 1		8	3	10^{-2}
Parameter 3 Differential Doppler	D			24	3	1
Parameter 4 Rotating doppler	D			24	3	1

4. SPACECRAFT ORIENTATION REQUIREMENTS (Outline spacecraft attitude control requirements, pointing accuracy and stability tolerances below)

A Spacecraft pointing accuracy (pitch, roll, yaw) 0.5°

B Allowable spacecraft rate (pitch roll, yaw) Limitations imposed to maximum S/C angular excursion and rate by the mechanical solution that will be adopted to connect tether to STS.

C S/C attitude knowledge req. Stabilized platform outputs needed to perform deployment/retrieval of tetherd satellite.

D Orbital parameters required for effective instrument operation (explain) Orbital data required to relate wake to STS orbital position.

E Instrument operation period Deployment/retrieval of tetherd satellite will take about two hours for each direction that will be probed. While deployed, instr. is utilized 100% of time. Overall time utilization in 1 week-sortie: 30% of time.

F Standby period Standby period will be 70% of overall time in 1 week-sortie.

5. CONTROL REQUIREMENTS (Describe those needed by function)

Tether deployment/retrieval requires establishing a control loop that starts from such observables as wire tension and satellite position and controls the tether's configuration to optimize measurements' output and minimizes risk to STS.

6 DISPLAY REQUIREMENTS

Visual display of six AGC channels and six Phase-lock indications is required.

7 INSTRUMENT DEVELOPMENT INFORMATION (If available)

	COST	SCHEDULE
INSTRUMENT PRELIM DESIGN	100 K	6 Months
INSTRUMENT FINAL DESIGN, FABRICATION AND TESTING	? M	1½ Year

8 REMARKS (Additional comments on EMI, thermal and Contamination requirements and other support systems etc.)

The instrumentation used in the Doppler tracking Experiment MA-089 of the ASTP Mission could be the basis for the design of the instrumentation required by this proposed wake sounding.

AMPS EXPERIMENT OPERATIONAL REQUIREMENTS (EOR)

1. TITLE	DATE.
Meteor Gun	September 1975
	PREPARED BY Harold B. Liemohn

2. OBJECTIVE To determine atmospheric properties in the stratosphere using metal pellets fired by a gun on the AMPS Spacelab pallet.

Atmospheric reentry physics for small (10 gm) pellets moving at satellite speeds (6-8 km/sec) indicates that they become luminous (brighter than 10th magnitude) over several kilometers of trajectory at altitudes of 20-50 km. Actual brightness depends on such properties as pellet material, trajectory illumination, reentry speed, atmospheric density, and atmospheric temperature.

The principal objective is the study of atmospheric properties in the stratosphere which are not conveniently monitored by aircraft, balloons, or rockets. Repetitive firing of pellets are expected to provide useful data about spatial and temporal variations of temperature and density (and pressure). The duration of the ionization trail is probably too short to determine wind patterns from radar echoes, but the possibility remains to be analyzed.

Exotic pellet materials have not been explored yet, but they offer potential for long-lived luminosity and/or measurement of atmospheric constituent ratios through selective chemical interactions.

The fundamental physics of reentry bodies might be extended by control experiments. Much of the theory for natural meteor burnup (at 80-100 km altitudes) is based on empirical formulas that have been fitted to experimental data A variety of pellet shapes could be tested for their burn rates. Different materials might be used in a layered spherical pellet to ascertain ablation rates Finally spin stabilized and tumbling properties may be differentiated by suitable launch services (such as rifled or unrifled barrels).

3 INSTRUMENTS List by name the AMPS instruments required to support the experiment, the function(s) performed by each instrument and the experiment peculiar control functions and displays required

INSTRUMENTS REQUIRED: (Use IFRD title)	INSTRUMENT FUNCTIONS	CONTROLS AND DISPLAYS
Meteor Gun AMPS IFRD 3	Firing a variety of pellet shapes, sizes, and weights over a range of velocities (0.5-2 km/sec at muzzle) and directions (gimballed gun platform). The gun should be of recoilless design to avoid disturbing the attitude of Spacelab and the propellent should be noncontaminating (special explosives, compressed inert gas, expanding shell casings, or possibly electromagnetic).	Reloading mechanism and round counter Firing readiness and triggering Muzzle velocity through photocells Gimbal platform orientation
Ground or aircraft based optical sensors, such as rich-field telescopes with fast photographic emulsions or telephoto meteor cameras coupled to electronic image intensifiers.	To record the optical brightness of the artificial meteor trail which may be very dim and short-lived.	Communication link to Spacelab crew to confirm location of anticipated meteor burn.
Ground based radar	To measure the position and distortion of the ionization trail if it is sufficiently long lived.	Communication link to Spacelab crew and optical sensor crews.

ORBITAL CONDITIONS (Time of year, day, night, altitude, inclination, vehicle attitude, etc.)	TARGET CONDITIONS. (Describe location—lat., long.,— size, altitude, etc.)	CREW ACTIVITIES:	4 EXPERIMENT CONDITIONS For each of the experiment conditions, identify the necessary conditions or events which must occur to support the experiment. Present graphically, if possible on attached sheets
Initially the spacecraft orbit must allow pellet ejection over telescope systems in the Southwestern United States, including the adjacent ocean. Complete burnup of pellet material in the stratosphere is reasonably assured, but initial ejections should be over unpopulated areas for safety and to reduce background skylight.	Obviously weather conditions over the ground observing locations must be clear. Since telescope pointing cannot be altered rapidly, it will be necessary to prepoint the gun and fire with timing accuracy of 0.1 second. On the other hand, optical fields of view may vary considerably	Crew is responsible for properly pointing the gun and firing a sequence of pellets during traversal of target area. Communications with ground observatories are important throughout the flyover. Orientation of gun and fire	
Eventually an array of mobile ground cameras would be deployed to study the stratosphere at several latitudes and longitudes. Pointing of the gun must be known accurately to specify the precise location for the meteor light trail. Exact specifications remain to be calculated but are probably on the order of 0.1°. Location of the Spacelab at the times of ejection are also essential--probably to within a few kilometers.	depending on distance to meteor trajectory and angular field of lens, so that injection criteria are unresolved at present.	control should not require more than ten minutes (provided the entire vehicle does not need rotation) of attention from one crewman.	

5. REMARKS

List other constraints that might be useful in scheduling, support systems sizing, etc

This is a new concept. Only theoretical analysis of reentry physics has been developed.

Various firing mechanisms need to be explored before a prototype gun is developed.

AMPS INSTURMENT FUNCTIONAL REQUIREMENTS

PART I · **TECHNICAL INFORMATION** H. B. Liemohn

1. TITLE Meteor Gun

DATE PREPARED 2/5/75

2. OBJECTIVE

To determine atmospheric properties in the altitude range 20-50 km by ejection of metal pellets from Spacelab.

3 DESCRIPTION (Outline operational modes, briefly describe equipment. Include sketch and/or block diagrams, showing required interfaces with other systems, whenever possible, as an attachment to this form.)

A recoiless repetitive firing mechanism that produces muzzle velocities of 0.5-2 km/sec for 10 gm pellets needs to be developed. Firing energy may be achieved by compressed gas, expanding shell casings, or selected explosives that do not contaminate the spacecraft environment. Atmospheric reentry at satellite speeds allows the pellet to be luminous (brighter than 10th magnitude) over several kilometers of trajectory at altitudes of 20-50 km. Brightness depends on atmospheric density and temperature as well as pellet material.

PART II **ENGINEERING INFORMATION**

1. WEIGHT, SIZE, AND LOCATION (Give estimated weight, size and location of completed experimental hardware, including unique cabling, plumbing, and support structure.)

EQUIPMENT ITEM	WEIGHT	VOLUME (m^3)		DIMENSIONS (m)		LOCATION EG PRESS, MODULE, PALLET, SUBSAT, ETC
		STORED	OPERATION	STORED	OPERATION	
Subsystem 1 Subsystem 2 Subsystem 3 Etc	~40kg	0.5m		1mx1mx0.5m		Spacelab pallet
TOTAL		or less		or less		

2 **POWER** (Provide requirements to be supplied by S/C for each subsystem or component in Item 1 above If power consumption not constant state requirements in enough detail so power profiles can be determined Indicate if there are any special requirements for power or voltage to be provided by the instrument

TOTAL S/C POWER REQUIRED (W)	Standby 10 Watts		Average	100 W Maximum
	VOLTAGE/POWER REQUIRED BY SEPARATE ASSEMBLIES			
	Voltage (V)	Power (W)	Power (W)	Power (W)
Subsystem # 1	Depends on	Standby	Average	Maximum
Subsystem # 2	firing	Standby	Average	Maximum
Subsystem # 3	mechanism	Standby	Average	Maximum

3 **DATA MEASUREMENT REQUIREMENTS** (State expected data and measurement characteristics in format specified below where applicable Include additional or different information as necessary)

SCIENCE OR HOUSEKEEPING PARAMETERS TO BE MEASURED	TYPE (DIGITAL ANALOG)	BAND WIDTH OR FREQ RANGE (LOW TO HIGH, Hz)	AMPLITUDE (e g., 0-5 V)	ACCURACY OR WORD LENGTH	MEASMTS PER UNIT TIME OR NO OF CHANNELS	SAMPLING OR BIT RATE
Subsystem # 1 Name						
Parameter 1 Loading Mechanism					DATA REQUIREMENTS UNKNOWN AT THIS TIME	
Parameter 2 Firing Readiness						
Parameter 3 Fire Control						
Parameter 4 Round Counter						
Subsystem # 2						
Parameter 1 Photoelectric Cell #1						
Parameter 2 Photoelectric Cell #2						
Parameter 3 Muzzle Velocity Recorder						
Parameter 4 Firing Time Record						
Subsystem # 3						
Parameter 1 Fimbal Platform Orientation						
Parameter 2						
Parameter 3						
Parameter 4						

4 SPACECRAFT ORIENTATION REQUIREMENTS (Outline spacecraft attitude control requirements, pointing accuracy and stability tolerances below)

A Spacecraft pointing accuracy (pitch, roll, yaw) To be determined by ground telescope field of view - probably 0.1°

B Allowable spacecraft rate (pitch, roll, yaw) Unknown

C S/C attitude knowledge req Specified by pellet velocity vector.

D Orbital parameters required for effective instrument operation (explain) Location to within few kilometers

E Instrument operation period
Few minutes over ground observation zone

F Standby period
Most of orbit

5. CONTROL REQUIREMENTS (Describe those needed by function)

Orientation of gimbal platform

Loading and firing

Ground observing conditions

6 DISPLAY REQUIREMENTS

Pellet velocity and firing time to ground observatories

7. INSTRUMENT DEVELOPMENT INFORMATION (If available)

	COST	SCHEDULE
INSTRUMENT PRELIM DESIGN	Unknown	
INSTRUMENT FINAL DESIGN, FABRICATION AND TESTING	Unknown	

8. REMARKS (Additional comments on EMI, thermal and Contamination requirements and other support systems, etc.)

This is a new concept. Only theoretical analysis of reentry physics has been developed. Various firing mechanisms need to be explored before a prototype gun is prepared previous rocket experiments have used high velocity and allowed recoil.